Journal of Human Evolution 90 (2016) 55–73

Contents lists available at ScienceDirect

Journal of Human Evolution

journal homepage: www.elsevier.com/locate/jhevol

Fossil hominin radii from the Sima de los Huesos Middle Pleistocene site (Sierra de Atapuerca, Spain)

Laura Rodríguez [a, b, *], José Miguel Carretero [a, c], Rebeca García-González [a], Carlos Lorenzo [d, e, c], Asier Gómez-Olivencia [c, f, g], Rolf Quam [c, h, i], Ignacio Martínez [c, j], Ana Gracia-Téllez [c, k], Juan Luis Arsuaga [c, l]

[a] Laboratorio de Evolución Humana, Dpto. de Ciencias Históricas y Geografía, Universidad de Burgos, Edificio I+D+i. Plaza Misael de Bañuelos s/n, 09001 Burgos, Spain
[b] Centro Nacional de Investigación sobre la Evolución Humana (CENIEH), Paseo Sierra de Atapuerca s/n, 09002 Burgos, Spain
[c] Centro UCM-ISCIII de Investigación sobre Evolución y Comportamiento Humanos, Avda. Monforte de Lemos, 5 (Pabellón 14), 28029 Madrid, Spain
[d] Institut de Paleoecologia Humana i Evolució Social (IPHES), Marcel·lí Domingo s/n, 43007, Tarragona, Spain
[e] Área de Prehistoria, Facultat de Lletres, Universitat Rovira i Virgili, Av. Catalunya, 35, 43002 Tarragona, Spain
[f] Dept. Estratigrafía y Paleontología, Facultad de Ciencia y Tecnología, Euskal Herriko Unibertsitatea, UPV-EHU, Apdo. 644, 48080 Bilbao, Spain
[g] IKERBASQUE, Basque Foundation for Science, USA
[h] Dept. of Anthropology, Binghamton University (SUNY), Binghamton, NY 13902-6000, USA
[i] Division of Anthropology, American Museum of Natural History, New York, NY 10024-5192, USA
[j] Área de Antropología Física, Departamento de Ciencias de la Vida, Universidad de Alcalá Campus Universitario, 28871 Alcalá de Henares, Spain
[k] Área de Paleontología, Departamento de Geología, Geografía y Medio Ambiente, Universidad de Alcalá, Campus Universitario, 28871 Alcalá de Henares, Spain
[l] Departamento de Paleontología, Facultad de Ciencias Geológicas, Universidad Complutense de Madrid, Ciudad Universitaria s/n, 28040 Madrid, Spain

ARTICLE INFO

Article history:
Received 3 November 2014
Accepted 15 September 2015
Available online 19 November 2015

Keywords:
Forearm
Homo
Neandertal
Cross-sectional properties
Iberian Peninsula

ABSTRACT

Complete radii in the fossil record preceding recent humans and Neandertals are very scarce. Here we introduce the radial remains recovered from the Sima de los Huesos (SH) site in the Sierra de Atapuerca between 1976 and 2011 and which have been dated in excess of 430 ky (thousands of years) ago. The sample comprises 89 specimens, 49 of which are attributed to adults representing a minimum of seven individuals. All elements are described anatomically and metrically, and compared with other fossil hominins and recent humans in order to examine the phylogenetic polarity of certain radial features. Radial remains from SH have some traits that differentiate them from those of recent humans and make them more similar to Neandertals, including strongly curved shafts, anteroposterior expanded radial heads and both absolutely and relatively long necks. In contrast, the SH sample differs from Neandertals in showing a high overall gracility as well as a high frequency (80%) of an anteriorly oriented radial tuberosity. Thus, like the cranial and dental remains from the SH site, characteristic Neandertal radial morphology is not present fully in the SH radii. We also analyzed the cross-sectional properties of the SH radial sample at two different levels: mid-shaft and at the midpoint of the neck length. When standardized by shaft length, no difference in the mid-shaft cross-sectional properties were found between the SH hominins, Neandertals and recent humans. Nevertheless, due to their long neck length, the SH hominins show a higher lever efficiency than either Neandertals or recent humans. Functionally, the SH radial morphology is consistent with more efficient pronation-supination and flexion-extension movements. The particular trait composition in the SH sample and Neandertals resembles more closely morphology evident in recent human males.

1. Introduction

A distinctive radial morphology in Neandertals was recognized more than 100 years ago (Gorjanović-Kramberger, 1906; Boule, 1911). When compared to recent humans, the Neandertal radius

* Corresponding author. Laura Rodríguez, Laboratorio de Evolución Humana, Dpto. de Ciencias Históricas y Geografía, Universidad de Burgos, Edificio I+D+i, Plaza Misael de Bañuelos s/n, 09001 Burgos, Spain.
E-mail addresses: lrgarcia@ubu.es, lrgagosto@gmail.com (L. Rodríguez).

http://dx.doi.org/10.1016/j.jhevol.2015.09.010
0047-2484/

has been described as more laterally curved, with a more medially oriented radial tuberosity and a longer neck length (Trinkaus, 1983; Trinkaus and Churchill, 1988; De Groote, 2011), and each of these traits has functional implications. A longer radial neck is related to a higher lever efficiency of the forearm (Trinkaus, 1983), while more medial orientation of the radial tuberosity and increased shaft curvature (which places the bone mass farther from the rotational axis) provide greater efficiency in pronation –supination (Trinkaus and Churchill, 1988; Galtés et al., 2008, 2009). Thus, the functional interpretation of this suite of anatomical features in the Neandertal radius is consistent with very powerful forearms and pronation-supination movements (Trinkaus and Churchill, 1988; De Groote, 2011). Fossil hominin radii can also provide useful information regarding manipulative abilities, complementing analyses of humeri (Trinkaus et al., 1994), scapulae (Carretero et al., 1997) and ulnae (Trinkaus et al., 1994; Churchill and Rhodes, 2009). In addition, it has long been argued that Neandertals have lower brachial indices than do modern humans, indicating a radius that is short relative to the humerus, perhaps reflecting adaptation to cold climates (Trinkaus, 1981), although this interpretation has been questioned (Holliday, 1999).

Prior to the Neandertals, radial remains attributed to the genus *Homo* are scarce (Tobias, 1978; Pearson and Grine, 1997; Carretero et al., 1999; Ward et al., 2015), and the phylogenetic polarity of some of these features remains to be clarified. Although incomplete, the Cave of Hearths (CH) radius combines thick cortical bone in its neck and shaft and a rather slender neck (as in archaic members of the genus *Homo*) with an anteromedially oriented tuberosity (as in modern humans) (Pearson and Grine, 1997). The Klasies River Mouth (KRM) radius also shows thick cortical bone in the radial neck, but, externally, the KRM radial neck is rather stout, resembling recent humans (Pearson and Grine, 1997). The Early Pleistocene radius from the site of the Gran Dolina (ATD6-43) in the Sierra de Atapuerca resembles recent humans in its anteriorly oriented radial tuberosity and relatively straight shaft, but departs from them in showing a long radial neck (Carretero et al., 1999). The Early Pleistocene radius KNM-ER 48100 suggests the presence of large-bodied individuals at this time period (Ward et al., 2015), while the incomplete SK 18b early *Homo* radius from Swartkrans in South Africa does not show a relatively slender neck (Tobias, 1978). A more medially oriented radial tuberosity is present in some early hominins, suggesting this may represent the primitive condition for the hominin clade (Carretero et al., 1999).

Given this dearth of radial fossils in the genus *Homo*, the site of the Sima de los Huesos (SH) in the Sierra de Atapuerca offers an important opportunity to study a large sample of Middle Pleistocene radii and to help clarify the phylogenetic polarity of radial features in the genus *Homo*. While the SH radii have been included in previous studies (Carretero, 1994; Carretero et al., 1999, 2012) they have not been fully described and analyzed. The principal aim of this study, then, is to present a complete inventory, morphological descriptions and metric analysis of the entire adult radial sample from the SH site.

The SH collection has increased significantly during years of controlled excavations, with more than 6500 human remains having been recovered to date. Careful restoration of the fossil collection over the years has resulted in the reconstruction of eight complete or nearly complete adult radii. Here we compare the SH radii with those of recent and Upper Paleolithic *Homo sapiens*, Neandertals and earlier fossil hominins to assess the phylogenetic polarity of some features. In addition, the cross-sectional properties of the radial diaphysis and neck, and their functional implications, are considered within a comparative framework.

2. Material and methods

2.1. The SH hominin radial sample

The Sima de los Huesos (SH) is a well-known Middle Pleistocene site in the Sierra de Atapuerca in northern Spain (Arsuaga et al., 1997a). The large sample of human remains represents at least 28 individuals of different ages and both sexes (Bermúdez de Castro et al., 2004) and represent the largest known repository of fossil hominins from the Middle Pleistocene. The SH hominin fossils have been recovered from a single stratigraphic level at the site (LU-6) and date to c.430 ky (thousands of years) ago (Arsuaga et al., 2014; Aranburu et al., in press). This new age estimate is internally consistent, revises previous ages proposed for the hominins (Bischoff et al., 1997, 2003; Arnold et al., 2014) and is congruent with the macro- and micro-mammal assemblages from the site (García et al., 1997; Cuenca-Bescós and García, 2007).

In addition to many primitive features, the SH hominins share some derived traits with Neandertals in the cranium and facial skeleton (Arsuaga et al., 1993, 1995, 1997b, 2014; Martínez and Arsuaga, 1997), dentition (Bermúdez de Castro, 1988; Bermúdez de Castro and Nicolás, 1995, Martinon-Torres et al., 2012), mandibles (Rosas et al., 2002) and postcranial skeleton (Arsuaga et al., 1991, 1995, 2015; Carretero, 1994; Carretero et al., 1997, 2004, 2005; Gómez-Olivencia et al., 2007; Bonmatí et al., 2010, Pablos et al., 2013, 2014). Based on these similarities, the SH hominins are considered to share a close phylogenetic relationship with the Neandertals (Arsuaga et al., 1991, 1997a,c, 2014; Carretero et al., 1997; Martínez and Arsuaga, 1997; Martinon-Torres et al., 2012).

The entire SH radial sample comprises 89 labelled fragments from both adult and subadult specimens. Of these, 49 labelled remains belong to adult individuals and are included in the present study. Some of these fragments fit together to comprise eight complete or virtually complete radii and portions of at least five other bones (Figs. 1–3). Taking into account the most frequently preserved region (the left midshaft), as well as size incompatibilities between specimens, we have determined that a minimum of seven adult individuals are preserved in the sample.

2.2. Comparative samples

For comparative purposes, we measured and analyzed a large sample ($n = 384$) of recent human adult radii of known sex and age housed at the University of Coimbra (Portugal) (Table 1). In addition, the Upper Paleolithic specimens from Abri Pataud, Dolní Věstonice and Pavlov were included. Our Neandertal sample is based on observations of original specimens, high quality casts and data taken from the literature. We also included data on radii from the sites of Gran Dolina in Spain as well as the Cave of Hearths and Klasies River Mouth in South Africa (Table 1). Cross-sectional geometric properties of the SH radii were compared with additional modern human samples (San Pablo and Aranda de Duero) as well as a few Neandertal specimens.

2.3. Measurement definitions

Metric variables used in the present study (Fig. 4A) largely follow those defined by Martin and Saller (1957) and Maia Neto (1957). In order to calculate the radial curvature we defined three measurement points relying on digitized photos imported into the Autocad software program (Autodesk, USA). The point 0 is the point of intersection between the long axis of the neck and that of the diaphysis, taken in anterior view (Fig. 4A). Point A is defined as the point where a line perpendicular to the neck axis, with its origin in point 0, intersects with the lateral radial margin. Point B is defined

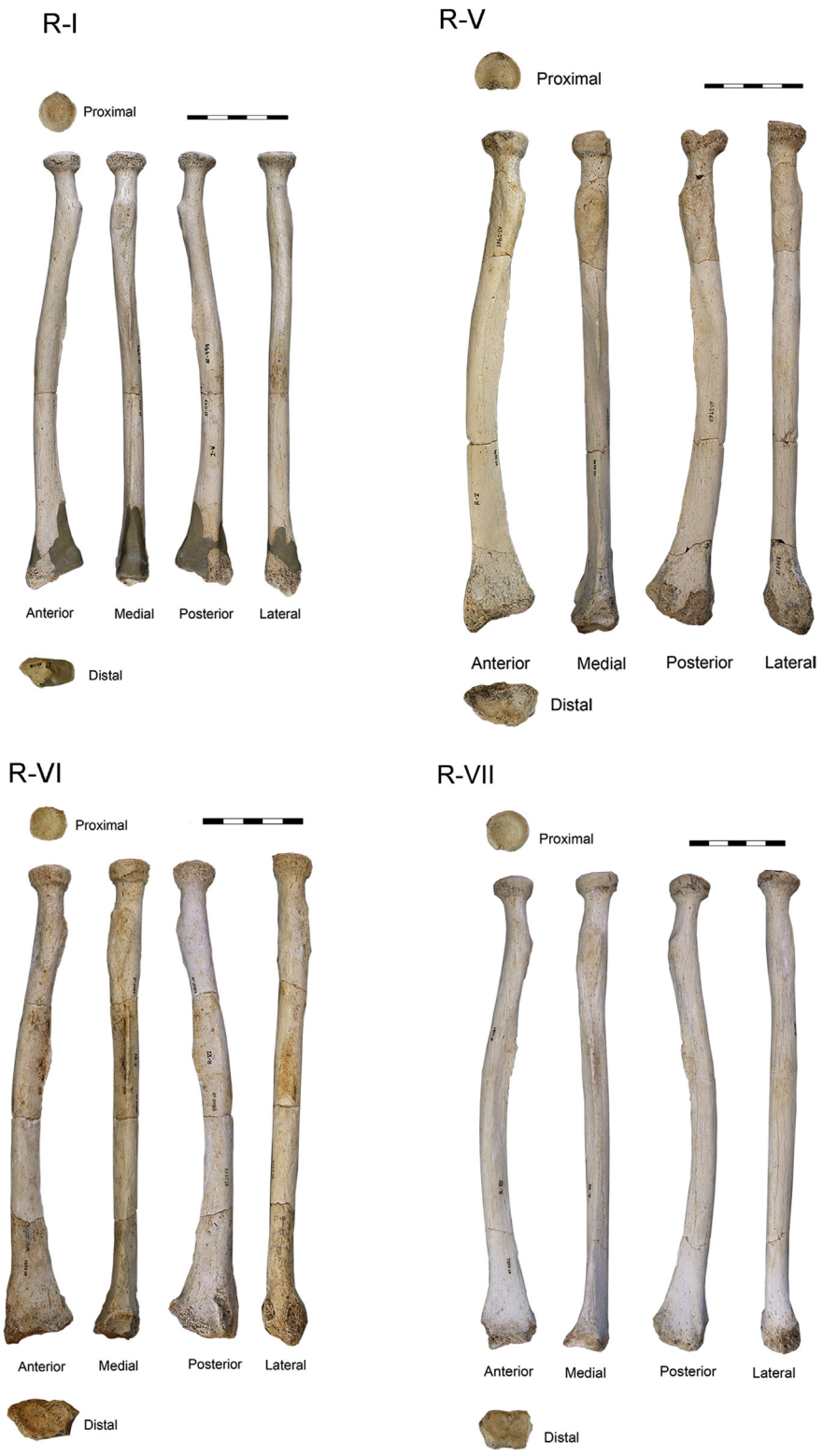

Figure 1. The Atapuerca (SH) complete adult right radii. (Scale bars = 5 cm.)

as the point along the lateral radial margin where the distal epiphysis begins to expand. The AB line is the chord of the shaft (M-6). The subtense of the shaft (M-6.1) is defined as the perpendicular distance from the AB line to the point of maximum curvature of the radial shaft along its lateral margin. To undertake these measurements on the complete specimens we used digitized photos imported into the Autocad software program (Autodesk, USA). Since the neck angle is defined as the angle formed by the diaphyseal and neck axes, a greater shaft curvature will tend to produce a more lateral projection of the radial diaphysis and a

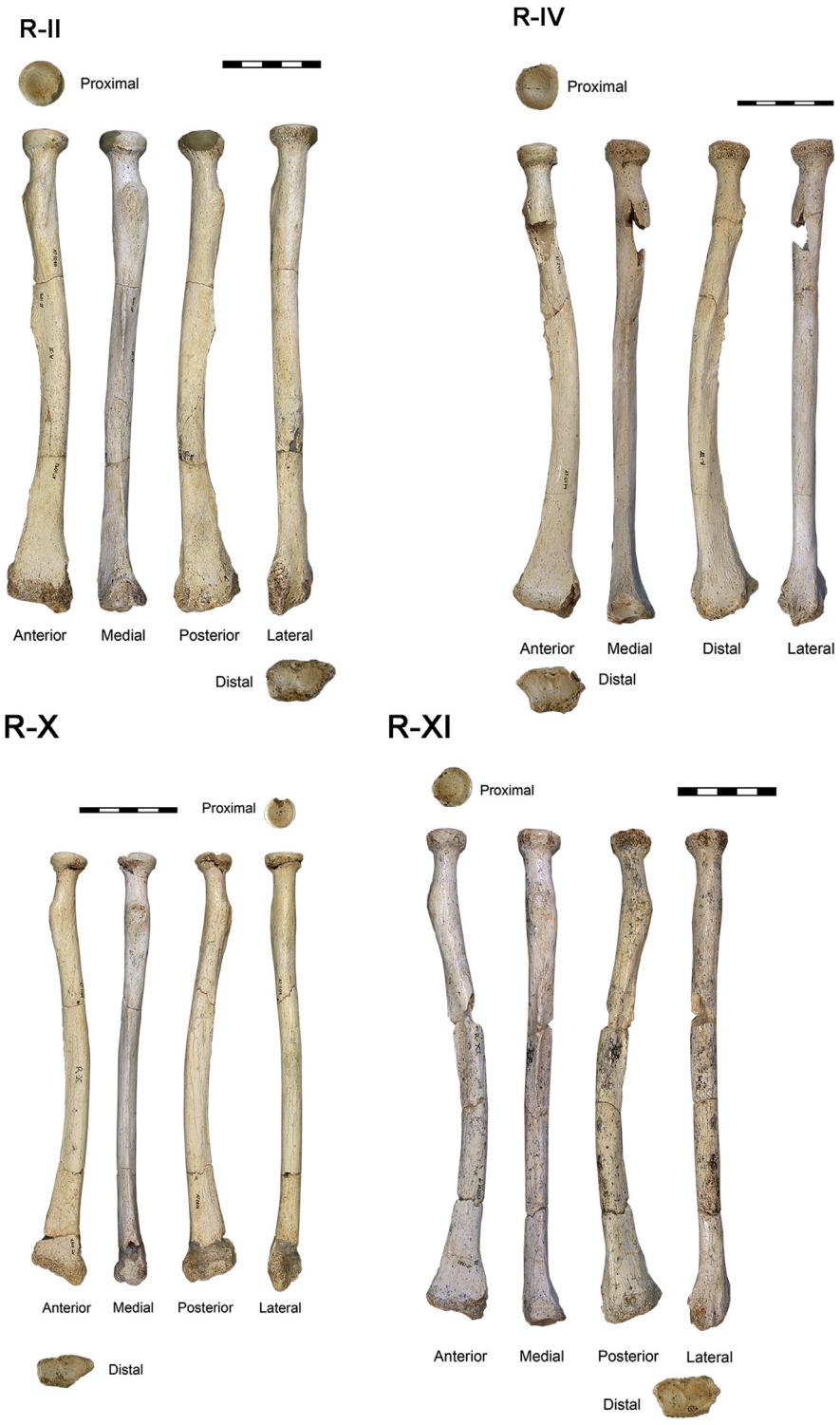

Figure 2. The Atapuerca (SH) complete adult left radii. (Scale bars = 5 cm.)

smaller neck angle (Trinkaus, 1983). In fact, the neck angle can be used to indirectly establish the shaft curvature in incomplete specimens.

2.4. Position of the radial tuberosity

We have established the position of the radial tuberosity (Fig. 4B) following the criteria outlined by Trinkaus and Churchill (1988), who defined five different states for the radial tuberosity position in relation to the long axis of the interosseous crest: 1) interosseous crest located posterior to the tuberosity; 2) interosseous crest located within the posterior third; 3) within the middle third; 4) within the anterior third of the tuberosity; 5) interosseous crest located anterior to the tuberosity. To simplify this, we grouped these five states into just two main categories: 1) radial tuberosity in an anterior position relative to interosseous crest (states 1–2 of

Figure 3. Incomplete adult radial remains from Atapuerca SH (scale bar = 5 cm): a) R-III; b) R-IX; c) R-XIV; d) AT-251; e) AT-343; f) AT-802; g and h) AT-4218+AT-4219; i) AT-5625+AT-5641.

Trinkaus and Churchill, 1988) and 2) radial tuberosity in a medial or posterior orientation relative to the interosseous crest (states 3–5 of Trinkaus and Churchill, 1988).

2.5. CT scanning parameters, cross-sectional properties and lever efficiency

Cross-sectional properties of the diaphysis and neck were calculated based on CT scans for all of the SH radii as well as the La Chapelle-aux-Saints and La Ferrassie 1 Neandertals and 82 recent human individuals (Table 1). CT scanning of the SH hominins and recent humans was performed at the University of Burgos (Spain) with a YXLON Compact X-Ray industrial multi-slice computed-tomography scanner. To obtain cross-sectional slices, the specimens were aligned along the bone's long axis with the radial head in a superior position. Scanner energy was 160 kV and 4 mA, slice thickness was collimated to 0.5 mm, inter-slice spacing was 0.5 mm, and the field of view was 18.52 cm with a reconstruction interval of 0.5 mm. Slices were obtained as a 1024 × 1024 matrix of 32 bit Float format with a pixel size of 0.18 mm.

Scanning parameters for the Neandertal individuals include the following: scanner energy = 140 kV and 3.5 mA, slice thickness = 1 mm and a field of view = 21.05 cm; slices were obtained as a 601 × 447 matrix, and the data were exported as dicom files.

The CT images were visualized using the commercially available software package Mimics™ (Materialise, NV, Belgium). Selected cross-sections were subsequently imported into Autocad (Autodesk, USA) to calculate total and cortical areas (*TA* and *CA*), which are related to axial strength, as well as the polar moment of inertia (*J*) which is a proxy for bone rigidity (Ruff, 2008). We also calculated second moments of inertia along the anteroposterior (AP), mediolateral (ML), maximum and minimum axes (*Ix, Iy, Imax,*

Table 1
Comparative samples used in the present study.

Specimen/sample	Sex	*n*	Species	Data source	Analysis[a]
Coimbra	Male	193	*H. sapiens*	Original specimens	TM
	Female	191			
San Pablo Medieval	Male	36	*H. sapiens*	Original specimens	CS
	Female	32			
Aranda de Duero	Male	14	*H. sapiens*	Original specimens	CS
Abri Pataud 26230A	Female?	1	*H. sapiens*	Original specimen	TM
Dolní Věstonice 3	Female	1	*H. sapiens*	Churchill (1994); Vleck (1997); Sládek et al. (2000)	TM
Dolní Věstonice 13	Male	1	*H. sapiens*	Churchill (1994); Vleck (1997); Sládek et al. (2000)	
Dolní Věstonice 14	Male	1	*H. sapiens*	Churchill (1994); Vleck (1997); Sládek et al. (2000)	
Dolní Věstonice 15	Male	1	*H. sapiens*	Churchill (1994); Vleck (1997); Sládek et al. (2000)	
Dolní Věstonice 16	Male	1	*H. sapiens*	Churchill (1994); Vleck (1997); Sládek et al. (2000)	
Pavlov 1	Male	1	*H. sapiens*		
Neandertal 1	Male	1	*H. neanderthalensis*	Cast	TM
La Ferrassie 1	Male	1	*H. neanderthalensis*	Original specimen	TM + CS
La Ferrassie 2	Female	1	*H. neanderthalensis*	Original specimen	TM
La Chapelle-aux-Saints 1	Male	1	*H. neanderthalensis*	Original specimen	TM + CS
Spy 1	Female	1	*H. neanderthalensis*	Cast	TM
Tabun C1	Female	1	*H. neanderthalensis*	Heim (1982)	TM
Shanidar 1	Male	1	*H. neanderthalensis*	Trinkaus (1983)	TM
Shanidar 4	Male	1	*H. neanderthalensis*	Trinkaus (1983)	
Shanidar 5	Male	1	*H. neanderthalensis*	Trinkaus (1983)	
Shanidar 6	Female	1	*H. neanderthalensis*	Trinkaus (1983)	
Shanidar 8	Female	1	*H. neanderthalensis*	Trinkaus (1983)	
Amud 1	Male	1	*H. neanderthalensis*	Cast; McCown and Keith (1939)	TM
Kebara 2	Male	1	*H. neanderthalensis*	Vandermeersch (1991)	TM
Krapina 189	Unknown	1	*H. neanderthalensis*	Original specimen	TM
Regordou 1	Unknown	1	*H. neanderthalensis*	Vandermeersch and Trinkaus (1995)	TM
ATD6-43	Unknown	1	*H. antecessor*	Original specimen	TM

[a] TM = traditional metric analysis; CS = cross-sectional analysis.

Imin) All geometrical properties and length dimensions were logarithmically transformed in order to avoid problems with different units of measurement (i.e. mm^4 versus mm).

The use of maximum radius length to establish the locations for calculating the cross-sectional properties (e.g. midshaft) may be problematic since Neandertals have longer radial necks than recent humans, in both absolute terms and relative to maximum bone length (Trinkaus, 1983; Carretero et al., 1999). Thus, to standardize the cross-sectional properties, we have designed a similar solution to that of Ruff and Hayes (1983) for the femur, and have divided the radial length into two different parts (the neck and the shaft). The radial neck (i.e. Fischer Neck length of Maia Neto, 1957) is defined as the distance from the upper limit of the medial margin of the radial head to the most proximal point of the radial tuberosity (Fig. 4A, measure FNL). The shaft length is defined by the diaphysis between the most distal point of the radial tuberosity and the tip of the styloid process. The geometrical properties (Fig. 4C) were calculated at the midpoint of the neck length (i.e. half of the Fischer Neck length) and at the midshaft of the diaphysis (as defined in the present study) and were then standardized by neck length and diaphyseal length, respectively. This same division of the radius into neck length and diaphyseal length also allowed us to analyze the lever efficiency (LE = FNL/Diaphyseal length) in the SH hominins, recent humans and Neandertals.

2.6. Bilateral asymmetry

Given the strong humeral diaphyseal bilateral asymmetry in Neandertals (Trinkaus et al., 1994; Trinkaus and Churchill, 1999), we also examined the possible existence of bilateral asymmetry in the radii, to ensure an accurate comparison of the SH radii cross sections. We calculated the asymmetry percentage for each individual and each cross-sectional property in our recent *H. sapiens* sample following the formula provided by Trinkaus et al. (1994):

$$\text{Individual asymmetry percentage} = [(\max - \min)/\min] \times 100$$

where max = the side with a higher value and min = the side with a lower value. In addition we performed a t-test between right and left radii in the entire recent human sample to provide a significance level to the asymmetry. We then divided the recent human sample into right and left radii for those variables (geometric properties) for which there was statistically significant bilateral asymmetry and compared only the corresponding side in the fossil specimens, that is, we analyzed the left and right sides separately.

2.7. Statistical analysis

Given the small sample size for the SH radii ($n = 8$), a univariate non-parametric Mann Whitney U test was performed in order to establish significant differences between samples. Sex assessment of the most complete radii has already been performed (Carretero et al., 2012). Due to the statistical problems arising when comparing samples through indices (Packard and Boardman, 1999), we used the analysis of covariance ANCOVA, which is a blend of two statistical procedures, regression and ANOVA. Regression removes effects of body size from the variable of interest and ANOVA then provides a sensitive test of the adjusted data (Packard and Boardman, 1999). Thus, ANCOVA evaluates whether the population means of a dependent variable are equal across levels of a categorical independent variable while statistically controlling for the effects of other continuous variables, known as covariates (Keppel, 1991). In the present study, ANCOVA was conducted when it was necessary to establish the effect of the factor (sample/species) on the relationship between two variables (dependent and covariable).

We have previously noted that size (sexual) variation in the SH hominins is similar to that of recent humans (Arsuaga et al., 1997b; Lorenzo et al., 1998). In our recent human sample, we explored the sex-related variation in several traits. Categorical principal component analysis (CATPCA) was used to analyze the association between different variables (robusticity, neck length, curvature and sex). It is preferred over correspondence analysis because, although they are conceptually the same, CATPCA is more robust with ordinal variables. The CATPCA procedure simultaneously quantifies categorical variables while reducing the dimensionality of the data variables. In order to do so, each original variable is ranked in ascending order, according to its alphanumerical value. Then, cases are assigned to categories using intervals chosen by the researcher, relying on criteria outlined by Max (1960).

In the present study, the values of each index were grouped into five categories following a normal distribution. Shaft curvature categories were: very straight, straight, mildly curved, curved and very curved. Neck length categories were: very short, short, medium, long and very long. Robusticity categories were: very gracile, gracile, medium, robust and very robust. Sex categories were: male and female. In CATPCA, dimensions correspond to components (i.e., an analysis with two dimensions results in two components), and object scores correspond to component scores. For the application of this method, no distributional assumptions about the variables have to be made. This kind of analysis differs from classic principal component analysis in that the CATPCA analyzes the relationship among different categories of different variables (for example the relationship among high bone curvature, long neck length and high gracility) and not the variables themselves (curvature, neck length, gracility). Finally, we also assessed the indices for the fossil specimens to see which of the recent modern human categories they fell into. All statistical analyses were carried out using IBM SPSS Statistics v.21 software (IBM, 2012).

2.8. Preservation and morphological descriptions of the SH radii

All the labeled fragments are named as AT (i.e. Atapuerca SH) followed by an Arabic number (AT-795). We give a Radius number, represented by the letter R and a Roman numeral (R-I) only when the proximal third (including the radial tuberosity and origin of the interosseous crest) is present.

Taking into account shape and size incompatibilities we can tentatively suggest several associations between the more complete SH radii. These are: R-X and R-I, R-II and R-VI, R-III and R-XIV, R-IV and R-V, R-VII and R-XI. In addition, although no physical connection can currently be established, AT-251 (Right) and AT-802 (Left) are compatible in size with R-III (Right) and R-XIV (Left), respectively.

2.8.1. Radius I (R-I) (AT-795 + 1097 + 1118) (Fig. 1) This is a virtually complete right radius, showing a transverse break located just below the midshaft. Minor reconstruction was required for the distal diaphysis and epiphysis, but there is contact between the lateral portion of the distal epiphysis and the diaphysis. Compared to modern humans it can be described as very gracile, with a very long neck and a curved diaphysis. Its radial tuberosity faces anteriorly. The cross-section at the maximum interosseous crest development is teardrop in shape. The radial head is slightly eroded along the medial and posterior margins, although the measurements are not affected. The radial head shows slight signs of degenerative changes in the form of small pits on the preserved portion of the posterior border. On the distal articular surface, the articulation for the scaphoid is missing. This small

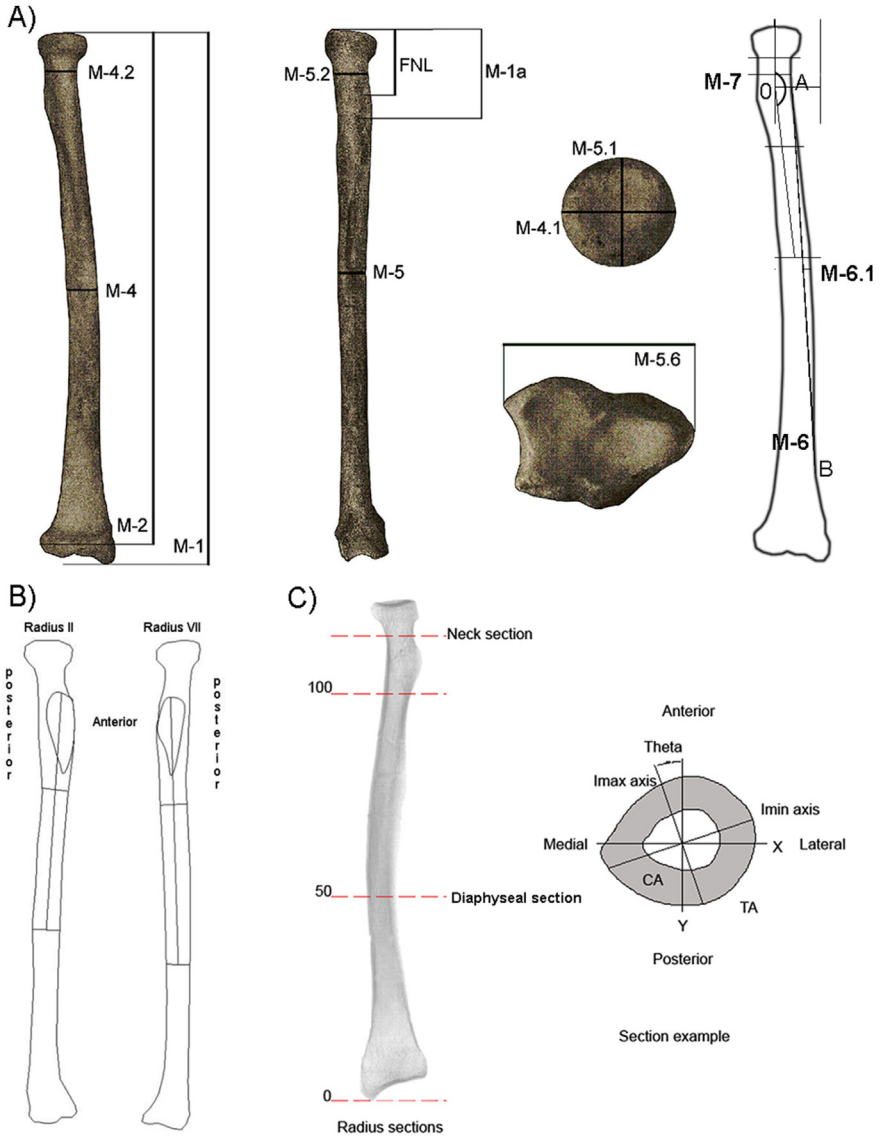

Figure 4. Measurements used in the present study. A) Metric variables. "M" = measurement taken according to Martin and Saller (1957), for curvature measurements explanation, please see text; "MN" = measurement taken according to Maia Neto (1957). See Table 1. B) Assessment of the position of the radial tuberosity in the SH sample showing a posterior position for Radius II and a medial position for Radius VII. C) Cross-sectional measurements of the radial diaphysis and neck. Data collection was limited to the midshaft position and the neck.

radius was considered to represent a female individual by Carretero et al. (2012).

2.8.2. Radius II (R-II) (AT-1090 + 1091 + 1092) (Fig. 2) This is a virtually complete left radius, comprising three labeled fragments. Only the posterior part of the radial head had to be reconstructed, and transverse breaks are located at the proximal and distal thirds of the shaft. Compared to modern humans, it can be described as having a very long neck but a similar degree of robusticity and shaft curvature. Its radial tuberosity is oriented anteriorly. The cross-section at the maximum interosseous crest development is teardrop shaped. The distal epiphysis, including the articular surface, shows well demarcated borders, and the dorsal tubercle is well-developed. This large specimen was considered to represent a male individual by Carretero et al. (2012).

2.8.3. Radius III (R-III) (AT-1260 + AT-1261) (Fig. 3a) This is the proximal third of a right radius from a small individual, formed by two labeled fragments. AT-1260 preserves the proximal epiphysis to the lower limit of the radial tuberosity. AT-1261 preserves the proximal diaphysis, from the radial tuberosity to the beginning of the interosseous crest. The radial head is slightly reconstructed on the posterior face. The radial tuberosity is oriented anteriorly and is stained with manganese oxide. There are no signs of pathology.

2.8.4. Radius IV (R-IV) (AT-2474 + 2493) (Fig. 2) This is a virtually complete left radius, lacking portions of the margin of the head and the distal portion of the radial tuberosity as well as the styloid process. It comprises two labeled fragments corresponding to the proximal third (AT-2493) and the distal two thirds (AT-2474). There also a slight loss of bone at the maximum point of interosseous crest development, although it can be seen that the cross-section is teardrop shaped. The styloid process and the crest for the brachioradialis muscle are missing. Compared to modern humans this specimen can be described as gracile, with a very long neck and very curved diaphysis. Its radial tuberosity faces anteriorly.

The distal articular surface shows well demarcated borders, and slight signs of degenerative changes are visible in the ulnar notch. This large specimen was considered to represent a male individual by Carretero et al. (2012).

2.8.5. Radius V (R-V) (AT-2498 + 2960 + 2961 + 3279) (Fig. 1) This is a virtually complete right radius, missing only a portion of the posterior margin of the head and a slightly eroded distal epiphysis. Transverse fractures are present at approximately the proximal and distal thirds of the diaphysis. Compared to modern humans it can be described as gracile, with a very long neck and a very curved diaphysis. The radial tuberosity is oriented anteriorly, and the crest for the brachioradialis muscle is strongly developed. The distal articular surface shows well demarcated borders. This large specimen was considered to represent a male individual (Carretero et al., 2012). Slight signs of degenerative changes are visible at the ulnar notch.

2.8.6. Radius VI (R-VI) (AT-2483 + 2488 + 2575 + 3277) (Fig. 1) This is a virtually complete right radius comprising four labeled fragments dividing the length into four similar segments, with transverse fractures separating them. The radial head is slightly eroded, with only the medial border being completely preserved. Compared to modern humans, this specimen can be described as having a longer neck and a more curved diaphysis but with a similar robusticity. The radial tuberosity is oriented anteriorly, and the cross-section at the maximum interosseous crest development is teardrop shaped. The distal epiphysis shows well-developed borders, and the ulnar notch shows signs of degenerative changes at its upper end. This large specimen was considered to represent a male individual by Carretero et al. (2012).

2.8.7. Radius VII (R-VII) (AT-3281 + 3282) (Fig. 1) This is a virtually complete right radius, lacking only the styloid process and comprising two labeled fragments. AT-3281 comprises the proximal three quarters, and AT-3282 represents the distal one quarter. Compared to modern humans, this specimen can be described as gracile, with a very long neck and very curved diaphysis. The radial tuberosity faces medially, and the cross-section at the maximum interosseous crest development is teardrop shaped. Unlike other SH specimens, the distal epiphysis does not show sharply demarcated borders. This large specimen was considered to represent a male individual by Carretero et al. (2012). There is no sign of pathology.

2.8.8. Radius IX (R-IX) (AT-2953 + 2959) (Fig. 3b) This specimen is represented by the proximal two thirds of the diaphysis, and comprises two labelled fragments. AT-2958 represents the proximal third, including the head and radial tuberosity, and is joined to the middle third (AT-2959) by a transverse fracture. Although incomplete, this specimen has the shortest absolute neck length (see Table 1) in the SH sample and the shaft is not markedly curved. The radial tuberosity is oriented anteriorly.

2.8.9. Radius X (R-X) (AT-1087 + 1109 + 2864) (Fig. 2) This is a virtually complete right radius comprising three labeled fragments. The radial head shows slight damage on the posterior margin and a small portion of the distal epiphysis had to be reconstructed. Compared to modern humans, this specimen is gracile, with a very long neck and a curved diaphysis. The radial tuberosity is oriented anteriorly. The cross-section at the maximum interosseous crest development is teardrop shaped and the crest is slightly broken at its proximal end. The distal articular surface shows well demarcated margins. This small specimen was considered to represent a female individual by Carretero et al. (2012). The radial head shows a slight degree of eburnation and pits in the fovea.

2.8.10. Radius XI (R-XI) (AT-1782 + 2032) (Fig. 2) This is a virtually complete left radius, lacking only a small part of the diaphysis near midshaft, part of the crest of the brachioradialis muscle, and showing slight erosion of the posterior border of the head. This specimen comprises two labeled fragments. AT-2032 represents the proximal three quarters and shows manganese staining, while. AT-1782 represents the distal quarter. Compared to modern humans it is gracile, with a long neck and a curved diaphysis. Its radial tuberosity is oriented medially. The cross-section at the maximum interosseous crest development is teardrop shaped. This large specimen was considered to represent a male individual by Carretero et al. (2012). There is no sign of pathology.

2.8.11. Radius XIV (R-XIV) (AT-1720) (Fig. 3c) This specimen is represented by the proximal third of a left radius, including the head, neck, tuberosity and part of the diaphysis of a small individual. Its radial tuberosity is oriented anteriorly. The radial head is eroded except on the medial border, and below the radial tuberosity only the posterior face of the diaphysis is preserved. There is no sign of pathology.

2.8.12. AT-251 (Fig. 3d) This small specimen comprises the complete distal epiphysis and only a very small portion of the right diaphysis, reaching its highest point along the lateral margin. The epiphyseal line is still visible and the distal articular surface shows well demarcated borders. There is no sign of pathology.

2.8.13. AT-347 (Fig. 3e) This specimen is a fragment of the middle portion of the right diaphysis, preserving part of the interosseous crest below the nutrient foramen.

2.8.14. AT-802 (Fig. 3f) This small specimen comprises the complete distal epiphysis and only a very small portion of the left diaphysis, reaching its highest point along the medial margin. The distal articular surface shows well demarcated borders. There is no sign of pathology.

2.8.15. AT-3865 + 4282 (Fig. 3g) This large specimen comprises two fragments of the left distal epiphysis, including the ulnar notch and the styloid process.

2.8.16. AT-4218 + AT-4219 (Fig. 3h) This is the anterior half of a left radial head from a large individual. There is no sign of pathology.

2.8.17. AT-5625 + AT-5641 (Fig. 3i) This specimen preserves approximately the middle third of a right radius, including most of the diaphysis, but missing the head, tuberosity and distal epiphysis. The nutrient foramen is not preserved, but the cross-section at the maximum development of the interosseous crest is teardrop shaped. Some manganese staining is present on the anterior aspect, but there are no signs of pathology.

3. Results

3.1. Metric analysis

In absolute dimensions (Table 2), the SH radii are significantly longer, have longer and anteroposteriorly-compressed necks and a greater curvature (larger diaphyseal subtense) in comparison to those of recent humans (Tables 3 and 4). On the other hand, compared to Neandertals, the only significant difference we found was in the ML diameter of the neck (Table 4), which is larger in the SH hominins.

Within the SH sample, shaft curvature, measured as the relationship between radial subtense and chord, varies from mildly curved to very curved (Table 5). A high frequency of curved diaphysis (Fig. 5A and Table 6) is shared with Neandertals. While considerable overlap between fossil and recent humans exists in the diaphyseal chord, the subtense values of most of the SH hominins and Neandertals is clearly higher than in recent humans, with several fossil specimens falling outside of the 95% equiprobability ellipses for recent humans (Fig. 5A). Although, as a sample, there is a statistically significant difference in curvature between SH hominins and modern humans (Table 7), some variation is

Table 2
Measurements of the Atapuerca (SH) radii.[a]

Side	RI	RII	RIII	RIV	RV	RVI	RVII	RIX	RX	RXI	R-XIV
	Right	Left	Right	Left	Right	Right	Right	Left	Left	Left	Left
Maximum length (M1)	222.0	241.0		255.0	256.0	243.0	253.0		221.0	249.0	
Articular length (M2)	214.0	229.0		240.0	244.0	234.0	244.0		209.0	238.0	
Head AP diameter (M-5.1)	20.0	23.5	21.1	22.7	24.0	20.4	22.3	*19.7	18.9	21.1	*19.5
Head ML diameter (M-4.1)	18.8	22.9	20.3	21.1	23.7	20.7	21.0	20.5	18.1	*19.9	*18.7
Head circumference (M-5.3)	60.0	74.0	65.0	73.0	75.0	65.0	70.0	*66.0	59.0	66.0	*61
Head-tuberosity length (M1.a)	37.0	43.0	34.0	41.8	44.3	39.3	41.4	36.1	38.3	40.2	40.5
Fischer Neck length (FNL)	23.8	25.8	23.2	28.3	27.1	24.0	30.6	21.5	24.0	30.3	22
Neck circumference (M-5.4)	33.0	43.0	38.0	43.0	43.0	42.0	38.0	41.0	37.5	40.0	37
Neck AP diameter (M-5.2)	10.5	13.0	11.9	12.9	13.6	13.1	12.5	12.6	10.6	12.5	11.1
Neck ML diameter (M-4.2)	9.7	12.4	11.0	11.9	12.6	12.3	11.1	12.3	9.2	11.2	9.9
Midshaft ML diameter	13.9	17.9		*16.7	17.8	17.8	15.6	17.6	12.6		
Midshaft AP diameter	9.9	12.5		12.4	13.1	12.7	13.6	10.7	9.6	*12.4	
Interosseous crest ML diameter (M4)	12.6	14.9		14.4	17.8	16.5	14.2	15.5	12.6	13.4	
Interosseous crest AP diameter (M5)	9.9	12.3		*12.4	12.9	12.8	13.9	10.7	9.6	12.3	
Shaft minimum circumference (M3)	34.0	43.0		42.0	43.0	43.0	42.0	40.0	34.0	40.0	
Minimum upper shaft circumference	34.0	43.5		44.0	46.0	43.5	42.0	39.0	34.0	40.0	
Distal epiphyseal breadth (M-5.6)	30.0	34.0		37.0	36.0	37.0	32.0		28.0	33.0	
Diaphysis subtense (M-6)	5.5	4.7		8.5	8.4	6.1	9.6		6.8	8.9	
Diaphysis chord (M-6.1)	157.0	160.0		191.5	200.3	169.7	184.5		160.4	177.9	
Neck angle (M-7)	165.0	171.0	165.0	171.0	169.0	166.0	165.0	157.0	168.0	165.0	166.0
Robusticity index (M3/M2)	15.9	18.8		17.5	17.6	18.4	17.2		16.3	16.8	
Interosseous crest index (M5/M4)	127.3	121.1		116.1	138.0	128.9	102.2		131.3	108.9	
Head (Apd)-length index (M4.1/M2)	8.8	10.0		8.8	9.7	8.8	8.6		8.7	8.4	
Head/neck index (M5.4/M5.3)	55.0	58.1	58.5	58.9		64.6	54.3	62.1	63.6	60.6	60.7
Martin length index (M1.a/M1	16.7	17.8			17.3	16.2	16.4		17.3	16.1	
Fischer Neck index (FNL/M2)	11.4	11.2		11.8	11.1	10.1	12.5		11.4	12.7	
Neck robusticity index (M5.2/M2)	4.9	5.7		5.4	5.6	5.6	5.1		5.1	5.3	
Head index (M4.1/M5.1)	94.0	97.4	95.2	93.0		101.5	94.2		95.8	94.3	95.9
Neck shape index (M4.2/M5.2)	92.4	95.4	92.4	92.2	92.6	93.9	88.8	97.6	86.8	89.6	
Distal epiphyseal index (M5.6/M2)	14.0	14.8		15.4	14.8	15.8	12.3		13.4	13.9	
Curvature index (M6/M6.1)	3.2	2.9		4.4	4.2	3.6	5.2		4.2	5.0	

[a] Linear measurements in mm. Neck angle in degrees. *Estimated measurement.

present within the SH hominins, as well as in the Neandertals. The Lower Pleistocene radius from Gran Dolina is very straight, in agreement with Carretero et al. (1999), with the subtense falling toward the lower limit of the recent human range of variation (Tables 5 and 6).

The neck angle can be used as an indirect indicator of shaft curvature, with lower angles indicating more curved shafts (Trinkaus, 1983). The mean neck angle of the SH radii (166.2°) is not different from that of Neandertals (166.8°) and both show a significantly smaller ($p < 0.01$) mean angle than the modern human sample mean from Coimbra (169.7°) (Table 3). Although not analyzed statistically, the mean values in several other recent human samples are even higher than the Coimbra mean (Fig. 5B). These results are consistent with the findings on shaft curvature reported above.

Shaft robusticity can be assessed by the robusticity index, which compares maximum length to the minimum shaft circumference (Martin and Saller, 1957). As a consequence of their length, the SH radial diaphyses are, as in Neandertals and *Homo antecessor*, gracile (slender) compared with fossil and recent humans (Table 3), although no statistical difference in robusticity was found between our modern human sample and SH (Table 7).

Regarding the radial head, there are no statistical differences in the anteroposterior (AP) and mediolateral (ML) diameters between any of the groups. Nevertheless, the AP diameter of the radial head in SH is slightly larger than the ML, similar to Neandertals (De Groote, 2011), but different from modern humans.

The SH radii have relatively longer necks than recent humans, with the same radial articular length (Fig. 6A). The same is true for the Neandertals (Trinkaus, 1983; De Groote, 2011), although Neandertals more often fall within the modern human range of variation. The robusticity index of the neck (defined as neck circumference versus neck length) (Fig. 6B; Table 3) and the head-neck index (Fig. 6C; Table 7), also indicate that the radial neck in both Neandertals and SH is more gracile than in modern humans.

On average, the SH radii have only a moderately projecting interosseous crest and a more rounded diaphysis than those of recent humans (Table 3). This is shared with Neandertals, the Middle Stone Age radius from Cave of Hearths (Pearson and Grine, 1997) and *H. antecessor* (Carretero et al., 1999).

Regarding the shape of distal epiphyses, no significant differences were found between the samples (recent humans, SH and Neandertals) in distal epiphyseal breadths, either absolutely or relative to maximum length (Tables 3 and 7). Nevertheless, the distal epiphysis of the SH radii is compressed in the AP direction compared with both fossil and recent *H. sapiens* (Table 7), which is probably related to the AP-compressed morphology of the bones of the first carpal row in the SH hominins (Lorenzo, 2007).

3.2. Position of the radial tuberosity

One of the most important functional traits in the radius is the position of the radial tuberosity. In the 10 SH adult radii in which the radial tuberosity orientation can be determined, it varies from anteromedially oriented ($n = 8$: R-I, II, IV, V, VI, VII, IX and X), similar to recent humans, to medially oriented ($n = 2$: R-VII and XI), which is the most common position in Neandertals. A medially positioned radial tuberosity is also found in the early hominin specimens A.L. 288-1p (*Australopithecus afarensis)* and KNM-ER 1500E (*Paranthropus boisei*), as well as the O.H. 62 individual *(Homo habilis)* (Trinkaus and Churchill, 1988) and at least one African Pleistocene radius (Cave of Hearths; Pearson and Grine, 1997).

Table 3
Descriptive statistics of radial variables in the SH hominins, modern humans and Neandertals.[a]

Variable name	SH (pooled sex)			Coimbra (pooled sex)			Neandertals (pooled sex)		
	Mean	S.D.	*n*	Mean	S.D.	*n*	Mean	S.D	*n*
Maximum length (M1)	242.5	14.0	8	226.1	16.3	456	233.3	14.8	13
Articular length (M2)	231.5	13.4	8	211.1	15.3	457	221.0	15.4	11
Head AP diameter (M-5.1)	21.1	1.5	9	20.6	2.0	388	21.4	2.4	12
Head ML diameter (M-4.1)	20.3	1.4	9	20.5	2.0	388	20.2	1.9	12
Head circumference (M-5.3)	66.4	5.2	9	64.5	6.4	388	65.0	5.8	7
Head-tuberosity length (M1.a)	39.8	2.7	9	31.4	3.1	458	31.7	1.7	5
Fischer Neck length (FNL)	25.7	3.2	10	21.1	2.5	458	22.6	1.3	4
Neck circumference (M-5.4)	39.9	3.3	10	41.5	4.6	459	37.2	3.5	8
Neck AP diameter (M-5.2)	12.3	1.0	10	13.7	1.7	460	12.1	1.6	11
Neck ML diameter (M-4.2)	11.4	1.2	10	12.0	1.4	460	10.3	0.8	12
Midshaft ML diameter	16.2	2.0	8				12.9		1
Midshaft AP diameter	11.9	1.4	9				14.7	0.1	2
Interosseous crest ML diameter (M4)	11.9	1.5	9	15.7	1.8	464	16.0	2.0	8
Interosseous crest AP diameter (M5)	14.7	1.8	9	10.9	1.3	464	10.6	1.5	8
Shaft minimum circumference (M3)	40.1	3.7	9	38.4	4.5	464	38.9	3.2	13
Minimum upper shaft circumference (F3)	40.7	4.3	9	38.5	4.1	464	40.0		1
Distal epiphyseal breath (M-5.6)	33.1	3.5	8	31.6	3.0	450	33.3	2.9	5
Diaphyseal subtense (M-6)	7.2	1.9	8	5.3	1.2	462	8.3	2.4	5
Diaphyseal chord (M-6.1)	175.2	16.0	8	168.0	13.4	462	170.2	12.9	5
Neck angle (M-7)	166.2	4.1	10	169.7	3.3	462	166.8	2.3	9
Robusticity index (M3/M2)	17.3	1.0	8	18.2	1.6	457	17.7	2.0	10
Interosseous crest index (M5/M4)	74.8	5.9	7	69.9	5.8	464	66.1	4.9	8
Head (Apd)- length index (M4.1/M2)	7.8	3.2	8	9.7	0.7	387	9.5	0.5	9
Head-neck index (M5.4/M5.3)	59.5	3.6	9	64.3	4.4	388	57.0	2.8	6
Martin length index (M1.a/M1	16.8	0.7	7	13.9	0.9	456	13.6	0.5	4
Fischer Neck index (F/M2)	11.5	0.8	8	10.0	0.9	457	10.5	0.4	4
Neck robusticity index (M5.2/M2)	5.3	0.3	8	6.5	0.6	456	5.7	0.6	9
Head index (M4.1/M5.1)	95.7	2.7	8	99.8	3.4	388	94.6	3.8	12
Neck shape index (M4.2/M5.2)	92.2	3.2	10	87.5	5.2	460	85.6	7.5	12
Distal epiphysis index (M5.6/M2)	14.3	1.1	8	15.0	1.0	447	15.2	1.4	4
Curvature index (M6/M6.1)	4.1	0.8	8	3.2	0.7	462	4.9	1.2	5

[a] Linear measurements in mm. Neck angles in degrees.

The Lower Pleistocene radius from Gran Dolina-TD6 (*H. antecessor*) shows an anteromedially facing radial tuberosity, as in recent humans (Carretero et al., 1999). Thus, the most frequent radial tuberosity orientation in the SH hominins is anteromedial and is shared by *H. antecessor* and *H. sapiens,* while there are also two SH radii in which the medially oriented condition is present (Figs. 1, 2 and 4B).

3.3. Cross-sectional properties and lever efficiency

The cross-sectional geometric properties for each SH radius and those of the comparative samples are given in Table 8. Since modern human radii show bilateral asymmetry in most of their cross-sectional geometric properties at the midshaft level (Table 9), we compared right and left radii separately. The radial midshaft in the SH hominins and Neandertals show thicker cortical bone (i.e. higher cortical area) than our recent comparative sample only for the left side (Fig. 7A, B). When the polar moment of inertia (*J*) is scaled to shaft length, the SH hominins and the two Neandertal specimens fall well within the range for recent humans with respect to their corresponding side (Fig. 7).

Although on average, the radial neck in the SH sample is more gracile externally than in the modern human sample (Tables 3 and 8), this is due primarily to their longer absolute length.

Table 4
Mann–Whitney U test results for radius variables.[a]

Variable	*H. sapiens* versus SH				*H. neanderthalensis* versus SH			
	H. sapiens Valid *n*	SH Valid *n*	U-value	*p*	*H. neanderthalensis* Valid *n*	SH Valid *n*	U-value	*p*
Max length (M1)	456	8	791.0	<0.01 (**)	8	13	33.0	0.17 (ns)
Head AP diameter (M-5.1)	388	11	1745.0	0.30 (ns)	11	12	65.5	0.97 (ns)
Head ML diameter (M-4.1)	388	11	2048.0	0.82 (ns)	11	12	57.0	0.57 (ns)
Fisher neck length (FNL)	458	11	602.5	<0.01 (**)	11	4	8.0	0.06 (ns)
Neck AP diameter (M-5.2)	460	11	1236.0	<0.01 (**)	11	11	59.5	0.94 (ns)
Neck ML diameter (M-4.2)	460	11	1907.0	0.16 (ns)	11	12	27.5	0.01 (**)
Interosseous ML diameter (M-4)	464	9	1541.5	0.17 (ns)	9	8	31.0	0.63 (ns)
Interosseous AP diameter (M-5)	464	9	1245.0	0.03 (*)	9	8	19.0	0.10 (ns)
Distal epiph. breadth (M-5.6)	450	10	1224.5	0.12(ns)	8	5	18.5	0.82 (ns)
Diaphyseal subtense (M-6)	462	8	753.0	<0.01 (**)	8	5	13.5	0.34 (ns)
Diaphyseal chord (M-6.1)	462	8	1426.0	0.27 (ns)	8	5	15.0	0.46 (ns)

[a] Measurements in mm. (ns) not significant; (*) $p \leq 0.05$; (**) $p < 0.01$.

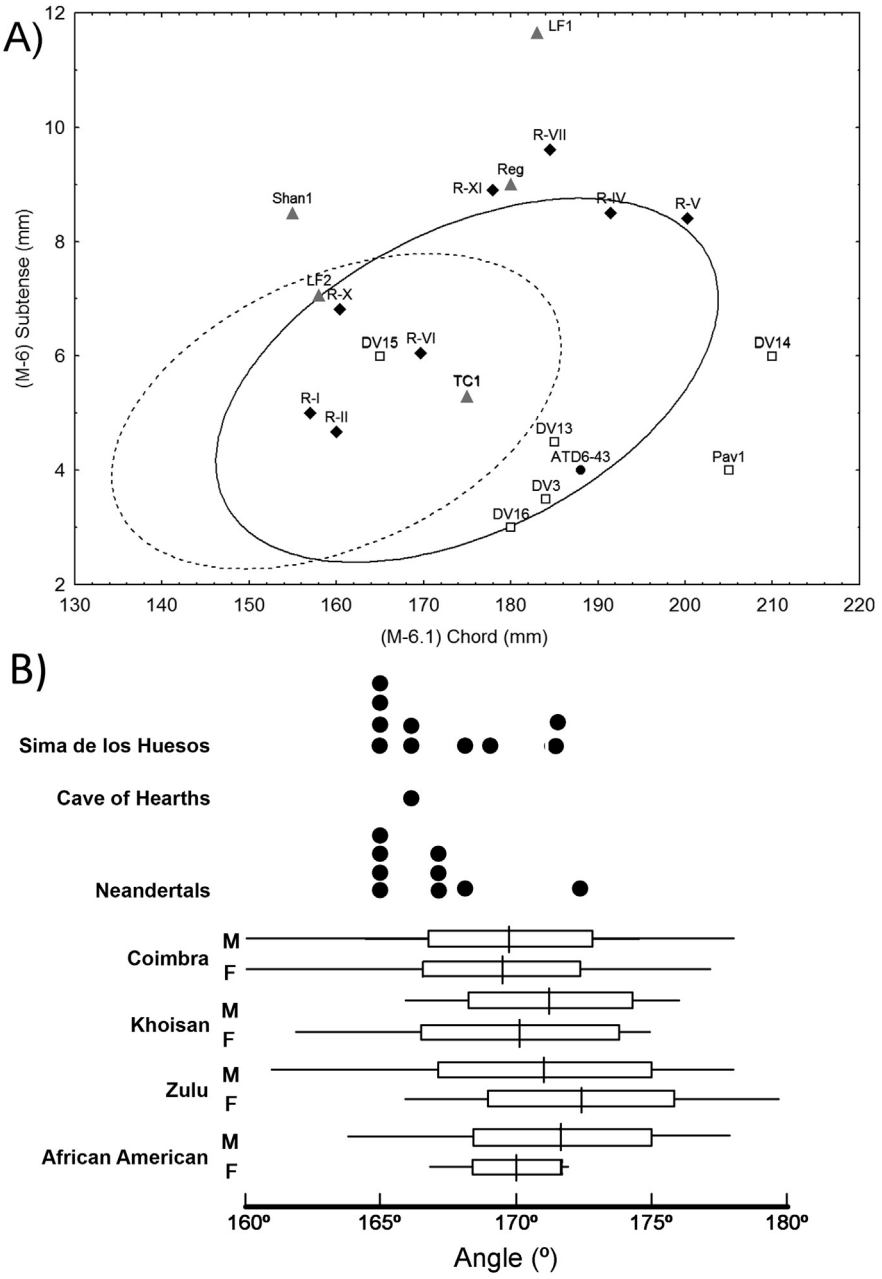

Figure 5. A) Scatterplot of the diaphyseal chord versus the subtense in recent and fossil hominins. The 95% equiprobability ellipse for modern human males (solid line) and females (dashed line) and the pooled sex regression line are also included. Black solid diamonds = SH hominins; gray solid triangles = Neandertals (N=Neandertal; R = Regourdou-1; LF1 = La Ferrassie 1; Spy1 = Spy 1; Shan1 = Shanidar 1); solid black dot: ATD6-43 = *H. anteccessor*. B) Neck angle in the SH sample, Neandertals and the Cave of Hearths specimen compared to several modern human samples. Recent human boxplots show the mean, the edges of the box represents two standard deviations and lines represent the range of values. Modern human (except Coimbra) and Cave of Hearths data extracted from Pearson and Grine (1997).

The SH hominins and Neandertals do not have thicker cortices in the radial neck than recent humans, although they generally fall within the upper half of the modern human range of variation (Fig. 8). In contrast, the Pleistocene *Homo* specimens from Cave of Hearths and Klasies River Mouth have thicker cortices than modern humans, falling well above the recent human range of variation (Fig. 8). Only a weak correlation ($r^2 = 0.39$; $p < 0.001$) was found between cortical area (*CA*) and total area (*TA*) in the neck. Since the ratio between *CA* and *TA* is related to axial loading strength, this may indicate that the radial neck does not undergo strong axial loadings, but, rather bending and torsion loadings.

When the polar moment of inertia (*J*) of the neck is scaled to neck length (Fig. 8B), the SH and Neandertal radii fall largely inside the modern human range of variation for *J*. However, the longer necks in some of the SH hominins (e.g. R-VII and R-XI), combined with similar values for *J*, indicate a weaker radial neck in some of the SH individuals (Radius IV, V, VII, XI) compared with recent humans. Neandertals and recent humans do not differ significantly in the general rigidity of the radial neck, (i.e. *J* versus neck length

Table 5
Frequency of appearance of radial traits in recent humans and fossil hominins.

	Category[a]	Values	Recent humans			Fossil hominins		
			%Pooled	%M	%F	%SH	%Nean	%ATD6
Sex	M		54.2	54.2				
	F		45.8		45.8			
Curvature	VST	1.5–2.3	14.4	12.3	16.8			100
	ST	2.4–2.8	16.9	17.8	15.9			
	MED	2.9–3.3	36.2	35.6	36.9	12.5	12.5	
	C	3.4–3.9	17.8	17.0	18.7	25.0		
	VC	4.0–5.5	14.8	17.4	11.7	62.5	87.5	
Neck length	VS	7.5–8.8	11.8	8.3	15.9			
	S	8.9–9.6	16.5	11.5	22.4			
	MED	9.7–10.2	42.4	42.7	42.1	12.5	33.3	
	L	10.3–11.0	14.1	17.8	9.8		33.3	
	VL	11.1–12.2	15.2	19.8	9.8	87.5	33.3	100
Robusticity	VG	14.2–16.1	15.4	5.9	26.6	12.5	12.5	100
	G	16.2–17.5	17.1	13.0	22.0	50.0	37.5	
	MED	17.6–18.7	38.8	41.1	36.0	37.5	25.0	
	R	18.8–20.1	12.0	14.2	9.4		25.0	
	VR	20.2–23.1	16.7	25.7	6.1			

[a] Category abbreviations:Sex: M = Male, F = Female.Shaft curvature categories: VST = very straight, VST = straight, MED = mildly curved, C = curved and VC = very curved.Neck length categories: VS = very short, S = short, MED = medium, L = long and VL = very long.Robusticity categories: VG = very gracile, G = gracile, MED = medium, R = robust and VR = very robust.

($p = 0.685$), while the SH sample is significantly weaker than recent humans ($p < 0.001$).

When the lever efficiency (LE) (the relative neck length, according to the lever law) is calculated, the SH hominins show a higher value (0.11) than recent humans (0.09) and Neandertals (0.10). These differences are statistically significant between recent humans and SH ($p < 0.01$) and SH and Neandertals ($p = 0.027$), but not between recent humans and Neandertals ($p = 0.071$).

3.4. Bilateral asymmetry

We used the degree of asymmetry found in the mid-shaft cross sectional parameters in modern humans and the suggested associations between right and left radii within the SH collection to examine bilateral asymmetry in the SH hominins. One association (R-VII and R-XI) shows a strong right side asymmetry (% asymmetry = 11.2 for *TA* and 7.7 for *CA*), while a second association (R-II and R-VI) shows a strong left side asymmetry (%

Table 6
Robusticity, neck length and curvature indices for fossil hominins and classification of the morphology compared to modern humans.

Sample	Specimen[a]	Sex[b]	Index values			Classification[c]		
			ROB	NECK	CURV	ROB	NECK	CURV
Sima de los Huesos	R-I	F	15.9	11.1	3.5	VG	VL	C
	R-II	M	18.8	11.3	2.9	N	VL	N
	R-IV	M	17.5	11.8	4.4	G	VL	VC
	R-V	M	17.6	11.1	4.2	N	VL	VC
	R-VI	M	18.4	10.3	3.6	N	L	C
	R-VII	M	17.2	12.5	5.2	G	VL	VC
	R-X	F	16.3	11.5	4.2	G	VL	VC
	R-XI	M	16.8	12.7	5.0	G	VL	VC
Neandertals	Chap	M	18.6	11.1	4.5	N	VL	VC
	LF1	M	17.2	10.0	5.6	G	N	VC
	Neand	M	19.5	12.3	5.3	R	VL	VC
	Keb2	M	17.4		5.5	G		VC
	SPY1	F	17.7	10.2	6.2	N	N	VC
	LF2	F	18.8	10.7	5.1	R	L	VC
	TC1	F	15.2		3.0	VG		N
	LQ5	?	17.2	11.7	6.4	G	L	VC
H. antecessor	ATD6-43		15.1	12.3	2.1	VG	VL	VST
Early Upper Palaeolithic modern humans	AP 26230A	F?	17.8	9.9	2.3	N	N	VST
	DV 3 (*)	F	15.6		1.9	VG		VST
	DV 13 (*)	M	17.7	9.7	2.6	N	N	ST
	DV 14 (*)	M	15.7	9.9	2.8	VG	N	ST
	DV 15 (*)	M	16.6	9.4	3.2	G	S	N
	DV 16 (*)	M	17.0	8.8	1.3	G	VS	VST
	Pavlov 1 (*)	?	15.5	9.5	1.9	VG	S	VST

(*) Data from Vleck (1997); Churchill (1994); Sladeck et al. (2000).
[a] La Chapelle-aux-Saints 1 (Chap); La Ferrassie 1 (LF1) and La Ferrassie 2 (LF2); Kebara 2 (Keb2); Neandertal (Neand); Spy 1 (SPY1); Tabun C1 (TC1); La Quina H5 (LQ5). *Homo anteccessor* ATD6-43; Early Upper Palaeolithic (EUP): AP (Abri Pataud) and DV (Dolní Věstonice) and Pavlov 1.
[b] Sex: M = Male, F = Female, ? = Sex unknown.
[c] See Table 5 for the values that define each category.

Table 7
Summarized ANCOVA results.

Variable	*H. sapiens* versus SH	
	B[(1)]	*p* value[(2)]
Curvature (Chord vs. subtense)	1.6	**<0.01**
Robusticity (Articular length vs. Shaft minimum circumference)	−1.4	0.214
Neck length (Articular length vs. Fischer Neck length)	3.3	**<0.01**
Head shape (ML vs. AP diameter)	0.9	**<0.01**
Head/neck (Neck perimeter vs. Head perimeter)	−0.3	**<0.01**
Distal epiphyseal shape	−3.5	**<0.01**

For variable definitions see Table 3. [(1)] Mean difference for the intercept between the SH hominins and modern humans. Positive values indicate SH > modern humans. [(2)] Values in bold are statistically significant.

asymmetry = 5.6 for *TA* and 11.0 for *CA*). A third association (R-I and R-X) shows more modest levels of left side asymmetry (% asymmetry = 3.7 for *TA* and 0.6 for *CA*), showing a similar level of asymmetry as in modern humans in TA but being almost symmetrical in CA.

3.5. Sexual dimorphism and categorical principal components analysis (CATPCA)

The first dimension of the CATPCA explains 39.0% of the total variance, with larger values along this dimension being related with a female classification (saturation = 0.80) and reduced robusticity (saturation = −0.77) (Fig. 9). The second dimension explains 26.8% of the total variance, with higher values along this dimension being related with reduced shaft curvature (saturation = −0.78) and longer necks (saturation = 0.61). Based on the separation of sexes along the first dimension, we can characterize modern human female and male radial morphologies. Modern male radii are generally more robust, with more curved shafts and longer necks, while modern female radii are generally more gracile, with less curved shafts and shorter necks. Intermediate categories for the morphological variables generally fall within the overlapping area that contains both males and females (Fig. 9).

Regarding the morphological traits defined above, the SH radii and those of Neandertals largely show a modern male-like morphology, with a more curved shaft and a longer neck length than recent modern humans (Table 6). While Neandertals have a mean robusticity index similar to that of recent humans (Trinkaus, 1983), the SH sample is more gracile and none of the SH specimens falls in the "robust" category for *H. sapiens*.

4. Discussion

4.1. Phylogenetic interpretation

The radial sample from the Sima de los Huesos site is an exceptional collection composed of 13 adult specimens, eight of which are complete or virtually complete. Thanks to the excellent preservation of the sample, we have noted that SH radii are morphologically different from those of recent humans and more similar to those of Neandertals. From a palaeobiological perspective, some of the radial features have been previously interpreted as Neandertal adaptations, and our analysis has shown that elements of Neandertal radial morphology were already present in the Middle Pleistocene hominins from Europe. In particular, the SH remains share with Neandertals a more elongated AP head, an absolutely and relatively longer radial neck, a more curved radial diaphysis and a more anteroposteriorly-compressed distal epiphysis. While the midshaft cross-section does shows a relatively thicker cortical area than in recent humans, this difference in structural robusticity fades when standardized by shaft length. This is also the case for the La Ferrassie 1 and La Chapelle-aux-Saints 1 Neandertal radii in our analysis, as well as Neandertal humeral remains (Trinkaus et al., 1998).

Apart from those of Neandertals, complete adult *Homo* radii are extremely scarce in the fossil record. The oldest is that of ATD6-43 from the site of the Gran Dolina (Carretero et al., 1999). This specimen shows a relatively long neck and straight diaphysis, a moderately projecting interosseous crest and thus a rounder shape at the midshaft. This same suite of features is also found in the A.L. 288-1p specimen attributed to *A. afarensis* (Senut, 1981; Johanson et al., 1982). Thus, this would appear to represent the primitive condition in the hominin clade, and the SH morphological pattern would appear to be derived. However, the MH2 radius attributed to *Australopithecus sediba* has been described as curved and also shows a relatively short neck (Churchill et al., 2013). Thus, some variation appears to be present in the radial morphology of early hominins, complicating our understanding of the phylogenetic polarity of some of these features within the hominin clade.

Regarding the position of the radial tuberosity, most of the SH specimens (80%) have an anteriorly-oriented radial tuberosity that is similar to the most common placement in recent humans. Nevertheless, a few specimens (20%) show a more medially placed radial tuberosity, resembling the most common expression found among Neandertals. Some degree of variation is also present in both Neandertals and recent humans (Trinkaus and Churchill, 1988), and the main difference between these taxa is the frequency of each type. A medially positioned radial tuberosity is also found in the early hominin specimens A.L. 288-1p and KNM-ER 1500E as well as the O.H. 62 individual attributed to *H. habilis*, and Trinkaus and Churchill (1988) have suggested that a medially oriented radial tuberosity may have been the ancestral condition for the Neandertals. This medial orientation is also present in at least one African Pleistocene radius (Cave of Hearths; Pearson and Grine, 1997), but not in *H. antecessor* (ATD6-43). The Atapuerca evidence (Gran Dolina and SH) suggests that the development of the anterior position of the radial tuberosity relative to the interosseous crest in *H. antecessor* and the SH hominins may be a synapomorphy (shared with recent humans) while Neandertals display a reversal to the primitive condition. Among the radial features studied here, we have not yet detected any autapomorphic traits for the SH hominins.

4.2. Functional interpretation

Many of the radial features analyzed here have functional implications. The CATPCA analysis demonstrates that, for our

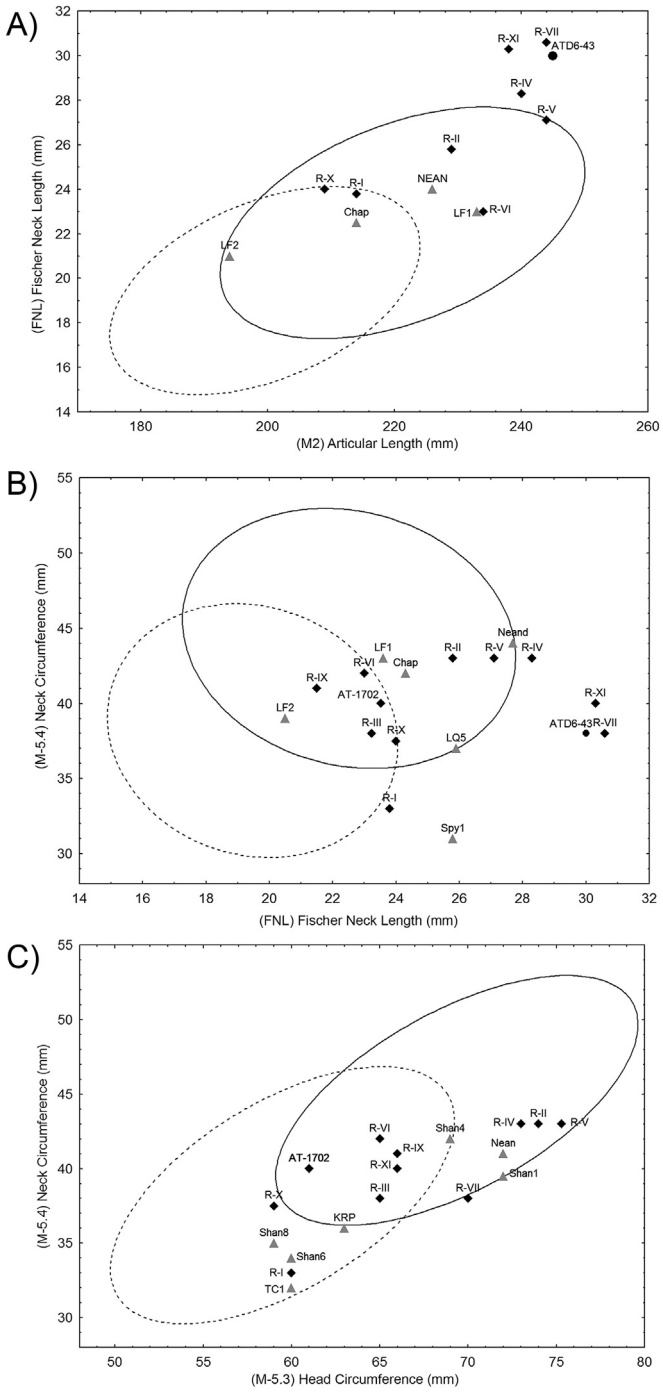

Figure 6. Neck length and robusticity for modern and fossil samples. A) Scatterplot of the Fischer Neck length versus articular length, showing the relative neck length. B) Scatterplot of the neck circumference versus Fischer Neck length, showing the neck robusticity and C) Scatterplot of the neck circumference versus head circumference, showing the relationship between the two measures. For all three scatterplots, the 95% equiprobability ellipse for modern human males (solid line) and females (dashed line) is presented. Black solid diamonds = SH sample; gray solid triangles = Neandertals (NEAN = Neandertal; REG = Regourdou; LF1 = La Ferrassie 1; LF2 = La Ferrassie 2, LCH = La Chapelle-aux-Saints; SPY1 = Spy 1; Shan1 = Shanidar 1; Shan4 = Shanidar 4; Shan5 = Shanidar 5; Shan 6 = Shanidar 6; Shan 8 = Shanidar 8; KRP = Krapina, Am1 = Amud 1).

Table 8
Cross-sectional geometric properties of the Atapuerca SH, Neandertal and modern human radii.[a]

Specimen	Side	Section	TA mm^2	CA mm^2	% CA	Ix mm^4	Iy mm^4	Imax mm^4	Imin mm^4	J mm^4	Zx mm^3	Zy mm^3
R-I	Right	50%	86.2	75.4	0.9	522.2	652.6	653.6	521.1	1174.7	87.6	131.0
		Neck	84.4	50.4	0.6	511.8	439.7	518.8	432.7	951.5	100.5	79.8
R-II	Left	50%	141.1	112.7	0.8	1449.2	1594.2	1637.6	1405.8	3043.4	203.2	232.1
		Neck	136.3	83.5	0.6	1405.4	1117.5	1413.1	1109.8	2522.9	208.1	158.7
R-IV	Left	50%	134.4	112.1	0.8	1148.3	1716.2	1730.8	1133.7	2864.5	146.6	282.7
		Neck	146.7	55.0	0.4	1177.4	921.1	1197.3	901.1	2098.5	175.7	122.7
R-V	Right	Neck	136.0	61.5	0.5	1065.0	949.9	929.8	1085.1	2014.8	159.7	130.0
R-VI	Right	50%	133.7	101.5	0.8	1189.8	1535.9	1581.5	1144.2	2725.7	154.8	236.5
		Neck	126.2	61.6	0.5	995.5	885.8	1042.1	839.3	1881.3	155.5	132.5
R-VII	Right	50%	130.6	115.8	0.9	1259.9	1459.6	1507.8	1211.7	2719.5	168.1	222.2
		Neck	111.7	77.5	0.7	967.6	838.4	1031.1	774.9	1806.0	164.0	130.2
R-X	Left	50%	89.4	75.8	0.9	547.9	713.3	725.7	535.5	1261.2	89.4	138.9
		Neck	85.0	58.3	0.7	569.0	472.0	574.7	466.3	1041.0	110.6	82.6
R-XI	Left	50%	117.5	109.0	0.9	1004.2	1193.1	1200.0	997.3	2197.3	150.3	204.6
		Neck	106.2	68.2	0.6	858.5	712.1	865.8	704.8	1570.6	149.0	114.8
La Ferrassie 1	Right	50%	110.3	81.8	0.7	796.8	1042.0	1042.9	795.9	1838.8	115.3	179.3
		Neck	115.7	57.3	0.5	821.6	788.5	942.4	667.6	1610.0	130.3	119.5
La Ferrassie 1	Left	50%	102.4	88.1	0.9	728.8	931.5	972.7	687.7	1660.4	115.1	165.6
		Neck	–	–	–	–	–	–	–	–	–	–
La Chapelle-aux-Saints	Right	50%	120.0	94.1	0.8	876.6	1429.1	1488.0	817.7	2305.7	108.8	241.2
		Neck	125.6	71.4	0.6	1159.0	856.7	1162.1	853.6	2015.7	184.6	127.0
Modern human left	*n*	50%	38.0	38.0	38.0	38.0	38.0	38.0	38.0	38.0	38.0	38.0
	Mean		108.4	81.2	0.8	765.0	1164.6	1166.0	737.3	1903.2	107.1	198.6
	sd		23.7	18.8	0.1	345.4	493.6	486.5	328.8	806.8	47.4	65.7
Modern human right	*n*	50%	29.0	29.0	29.0	29.0	29.0	29.0	29.0	29.0	29.0	29.0
	Mean		101.2	75.2	0.7	652.4	1046.1	1055.3	643.3	1698.6	85.0	188.5
	sd		27.4	20.6	0.1	413.2	649.7	661.9	400.9	1059.8	39.8	84.0
Modern human	*n*	Neck	67.0	67.0	67.0	67.0	67.0	67.0	67.0	67.0	67.0	67.0
	Mean		132.4	62.0	0.5	1111.4	935.9	1166.8	850.5	2017.3	165.3	133.1
	sd		24.9	16.0	0.1	444.2	393.9	474.1	380.4	837.2	47.6	46.6

[a] Please see text for variable definitions.

recent sample, a long neck and robust and curved diaphysis is associated mainly with males. By definition, this pattern provides mechanical advantages. Curved bones have been argued to represent an optimum response to both internal (muscle and weight) loadings and external loadings, due to the effect of carrying (Lanyon, 1980; Bertram and Biewener, 1988), and Frost (1973) established that morphological and experimental evidence tend to support that long bone curvature acts to improve loading predictability. Furthermore, a high diaphyseal curvature could result in more powerful rotational movements because the entire forearm bone mass is located farther from the axis of rotation (Yasutomi et al., 2002; Galtés et al., 2008, 2009). A longer neck is related to optimal pronation-supination, and to the mechanical efficiency of the lever arm of the biceps brachii muscle, since radii with longer necks need a lower biceps brachii force (and thus lower stresses) to move the same weight (flexion and extension). Comparatively, all SH radii have a higher lever efficiency ($p < 0.001$) than recent humans and although also higher than in Neandertals, they are not statistically different ($p = 0.0532$).

Neandertals and SH share a more oval head in comparison with recent humans. It has already been shown that the AP head diameter relative to the ML diameter assists in pronation-supination movements (Kapandji, 1999; De Groote, 2011), and the SH hominins and Neandertals would have more efficient pronation-supination and flexion-extension movements. Some early hominins and *H. antecessor* have a relatively long neck but a straighter diaphysis, and their pronation-supination movement may not have been as efficient as in the SH hominins and Neandertals, but still higher than in modern humans. This could be related to the lever efficiency (see above) where radii with longer necks need a lower biceps brachii force (and thus lower stresses) to move the same weight (flexion and extension). Future analysis of the SH ulnae may make it possible to more fully characterize the functional implications of some of these radial features in forearm function, as demonstrated by De Groote (2011) for Neandertals. Given the similarity to the Neandertals in many radial features within the SH sample, forearm function may have also been similar between these two groups of hominins.

Table 9
Bilateral asymmetry in cross-sectional properties at midshaft and in the radial neck in the modern human sample.[a]

	Asymmetry (%)	Midshaft		Asymmetry (%)	Neck	
		T-value	*p*		*T-value*	*p*
Total Area	3.9	2.51	**0.02**	3.4	−0.88	0.39
Cortical Area	4.8	2.79	**0.01**	1.1	0.14	0.89
Ix	7.1	1.67	0.12	4.6	−0.49	0.63
Iy	13.3	2.45	**0.03**	1.7	−0.15	0.88
Imax	13.4	2.24	**0.04**	1.7	−0.53	0.60
Imin	8.9	2.09	**0.05**	4.7	−0.12	0.91
J	10.9	2.23	**0.04**	3.3	−0.34	0.74
Zx	4.0	−0.62	0.54	2.1	−0.17	0.87
Zy	11.2	2.96	**0.01**	1.0	−0.10	0.92

[a] Ix, Iy, Imax, and Imin = second moments of inertia along the anteroposterior (AP), mediolateral (ML), maximum and minimum axes respectively. J = polar moment of inertia. Percentage asymmetry was calculated, following Trinkaus et al. (1994), as the absolute difference between maximum and minimum values divided by the minimum value, and multiplied by 100. Values in bold indicate statistical significance ($p \leq 0.05$).

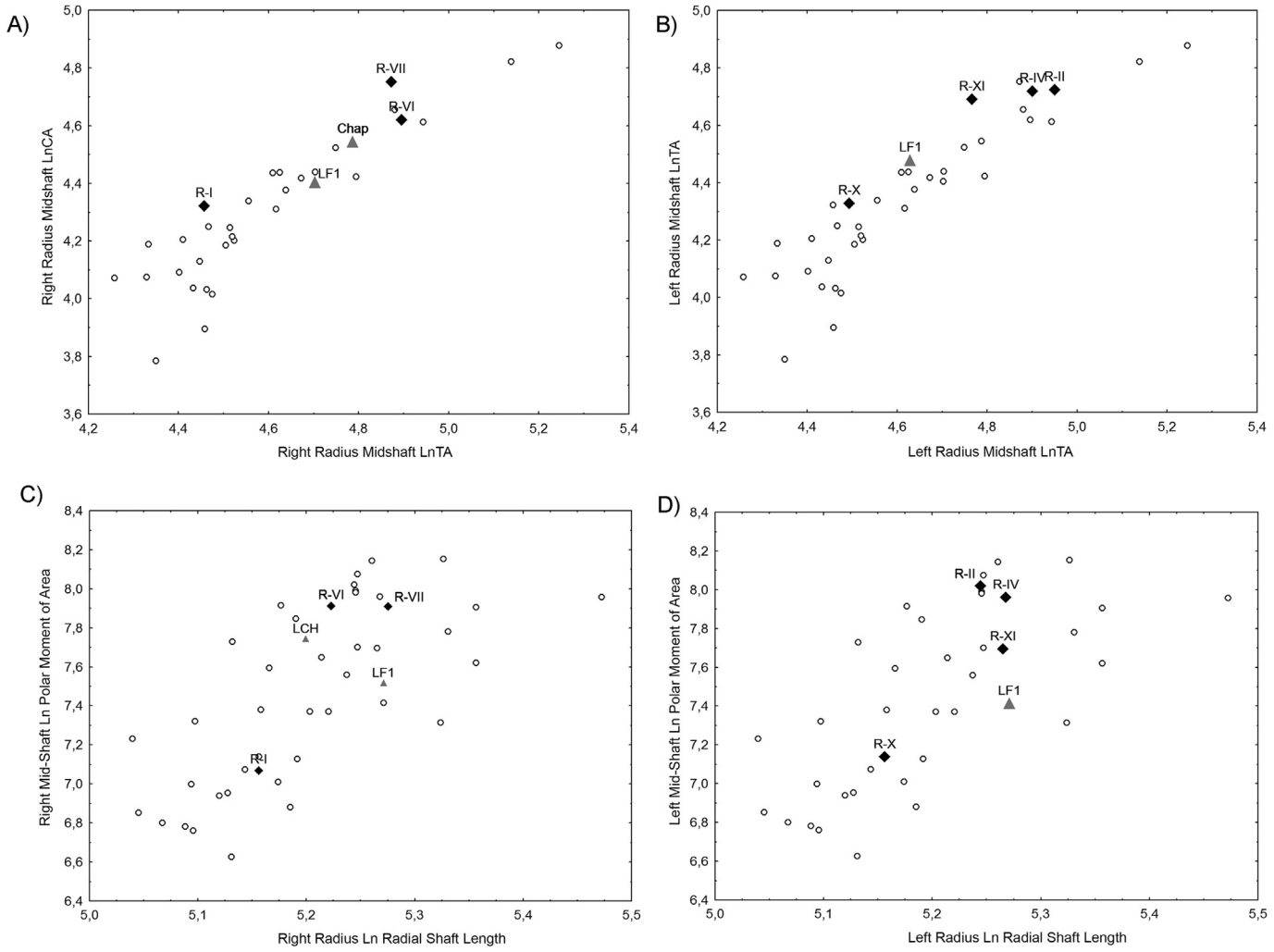

Figure 7. A–D. Scatterplots of logged (ln) midshaft geometric properties. Logged cortical area (lnCA) versus logged total area (lnTA) at midshaft in right (A) and left (B) radii. Logged midshaft polar moment of inertia (lnJ) versus logged shaft length in right (C) and left (D) radii. Open circle = modern sample. Black solid diamonds = SH. Gray solid triangles = Neandertals (LF1 = La Ferrassie 1, LCH = La Chapelle-aux-Saints).

4.3. Bilateral asymmetry

The presence of bilateral asymmetry in the human appendicular skeletal remains has long been recognized and there have been numerous attempts to quantify its level and direction, and to infer its significance (Trinkaus et al., 1994 and references therein). In this paper we have shown that there is statistically significant bilateral asymmetry in some of the cross-sectional parameters at the midshaft level of the radius in modern humans. Relying on the proposed associations between some of the SH radii, there are three pairs in which this cross-sectional parameter can be studied.

We have observed that one pair (R-VII + R-XI) has a strongly dominant right side, one has a strongly dominant left side (R-II + R-VI), and the third (R-I + R-X) shows less pronounced left side dominance. This is in contrast with the orientation of buccal striations on the teeth which suggested primarily right-handedness in the SH sample (Bermúdez de Castro, 1988; Lozano et al., 2009). There is also one association (R-VII + R-XI) that is strongly right-handed, and this strong laterality has also been shown in the cross-sectional properties of some Neandertal humerii (Trinkaus et al., 1994). Some degree of variation in the humeral asymmetry may be present between European Neandertals and those of southwest Asia, since higher degrees of laterality are found in La Chapelle-aux-Saints-1, Spy 2 and (less-so) La Ferrassie 1, while both Tabun C1 and Kebara 2 show asymmetry values which are within or close to the interquartile ranges of recent humans.

5. Conclusion

The SH radial remains are characterized by having a curved diaphysis, an absolutely and relatively long neck, as well as a more AP developed radial head, and in these features they are similar to the Neandertals. The main difference is the high frequency of an anteriorly oriented radial tuberosity in the SH hominins. In addition, some Neandertals can be classified as robust, but none of the SH radii falls into this category.

Further studies of the SH postcranial material will permit us to characterize the complete skeletal morphology of the Sima de los Huesos sample, more fully understand the degree of variation within the collection and analyze the functional implications. At

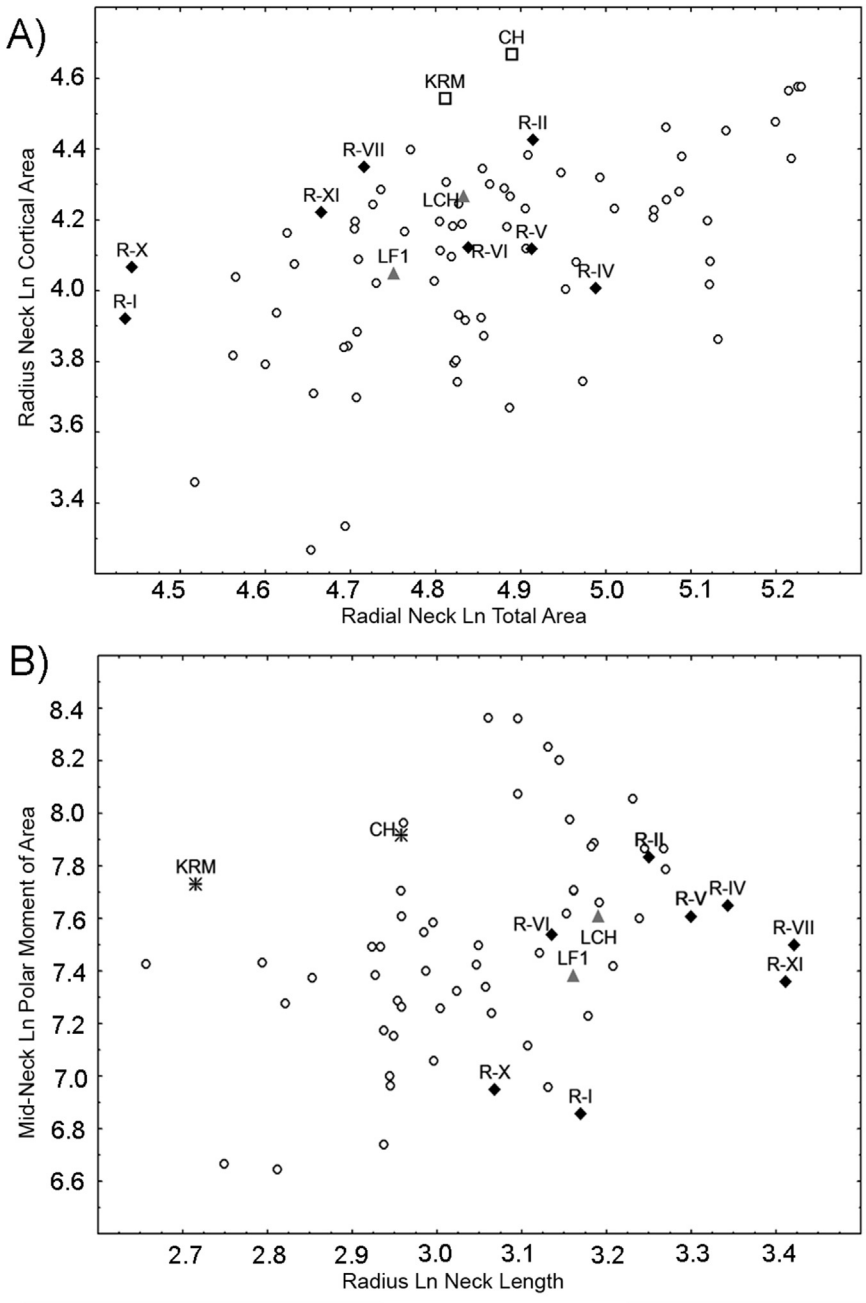

Figure 8. Scatterplot of cross-sectional geometric properties of the neck. A) Logged mid-neck cortical area versus logged mid-neck total area. B) Logged mid-neck polar moment of area versus logged radius neck length. Open circle = modern sample. Black solid diamonds = SH. Gray solid triangles = Neandertals (LF1 = La Ferrassie 1, LCH = La Chapelle-aux-Saints).

present, the SH postcranial evidence supports a close phylogenetic relationship between the SH hominins and Neandertals, as demonstrated by the cranial and dental evidence. Both the Middle Pleistocene SH hominins and the Early Pleistocene human fossils from Gran Dolina -TD6 (Carretero et al., 1999) are crucial to our understanding of human evolution in Europe. Interestingly, some differences are apparent in the radial features between these two sites, with the Gran Dolina specimen showing a very straight shaft. The data presented here can also shed light on the evolutionary continuity between Early and Middle Pleistocene populations in Europe.

More studies conducted on the SH postcranial material would permit us to characterize the complete skeletal morphology of the Sima de los Huesos sample and its variation and functional significance. At present, the SH postcranial evidence supports the phylogenetic relationship between SH and Neandertals demonstrated by the cranial and dental evidence. Both the Middle Pleistocene SH hominins and the Early Pleistocene human fossils from (Carretero et al., 1999) are crucial to our understanding of human evolution in Europe, but the continuity between Early and Middle Pleistocene populations in Europe is still subject to debate.

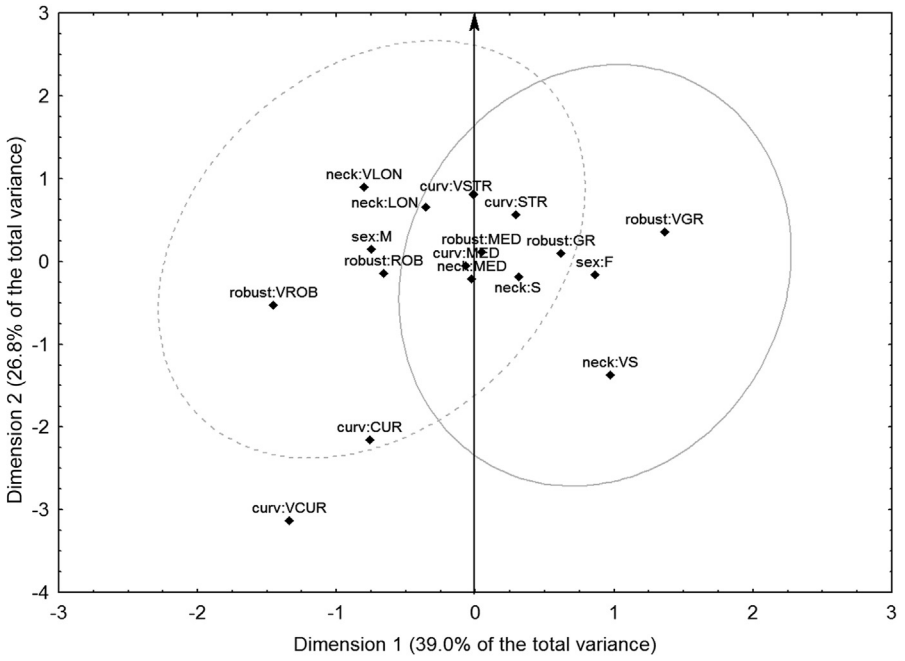

Figure 9. Categorical Principal Component Analysis (CATPCA) showing the relationship between selected morphological traits and sex in recent humans. Sex (M = male, F = female); Curv: curvature (VSTR = very straight, STR = straight, MED = medium, CUR = curved, VCUR = very curved); Robust: robusticity (VGR = very gracile, GR = gracile; MED = medium, ROB = robust, VROB = very robust); Fischer Neck length: neck (VS = very short, S = short; MED = medium, LON = long, VLON = very long).

Acknowledgements

We acknowledge the dedication of the Atapuerca research team during field and laboratory work. We have benefitted from discussions with our colleagues from the Centro Mixto UCM-ISCIII of Madrid and from the Laboratorio de Evolución Humana (L.E.H.) at the University of Burgos.

We are grateful to colleagues who gave us permission to access important skeletal collections in their care and kindly provided assistance: A. Froment, P. Mennecier, A. Fort, and A. Balzeau from Museé de l'Homme, Paris; Ana Luisa Santos and María Eugenia Cunha from Instituto de Antropologia de la Universidad de Coimbra; J. Radovcic from Croatian Natural History Museum of Zagreb. Special thanks to María Cruz Ortega for her careful restoration and preservation of the Atapuerca SH human fossils.

This research has received support from the Ministerio de Economía y Competitividad of Spain project N° CGL2012-38434-C03-01 (previous Projects CGL2006-13532-C01/02/03, CGL2009-12703-C03-01/02/03; 2009-SGR-2009-324) and by the Junta de Castilla y Leon projects No. BU032A06 and BU005A09. Field work at the Atapuerca sites is supported by the Junta de Castilla y León and Fundación Atapuerca.

L.R. received a grant from the Fundación Atapuerca and currently is funded by CPIN 03-461AA-692.01 project (Junta de Castilla y León, the European Social Fund). A.G.O had a Marie Curie IEF grant during part of this work and is currently also supported by the Gobierno Vasco/Eusko Jaurlaritza (Research Group IT834-13), and A.G.T has a Contract-grant from the Ramón y Cajal Program, RYC-2010-06152.

References

Aranburu, A., Arsuaga, J.L., Sala, N., 2015. The stratigraphy of the Sima de los Huesos (Atapuerca, Spain) and implications for the origin of the fossil hominin accumulation. Quatern. Int. in press, http://dx.doi.org/10.1016/j.quaint.2015.02.044.

Arnold, L.J., Demuro, M., Parés, J.M., Arsuaga, J.L., Aranburu, A., Bermúdez de Castro, J.M., Carbonell, E., 2014. Luminescence dating and palaeomagnetic age constraint on hominins from Sima de los Huesos, Atapuerca. Spain. J. Hum. Evol. 67, 85–107.

Arsuaga, J.L., Carretero, J.M., Martinez, I., Gracia, A., 1991. Cranial remains and long bones from Atapuerca/Ibeas (Spain). J. Hum. Evol. 20, 191–230.

Arsuaga, J.L., Martínez, I., Gracia, A., Carretero, J.M., Carbonell, E., 1993. Three new human skulls from the Sima de los Huesos Middle Pleistocene site in Sierra de Atapuerca, Spain. Nature 362, 534–537.

Arsuaga, J.L., Martínez, I., Gracia, A., Carretero, J.M., 1995. Los restos craneales y postcraneales de la Sima de los Huesos (Sierra de Atapuerca) y la evolución Humana en el Pleistoceno Medio/Cranial and postcranial remains at the Sima de los Huesos (Sierra de Atapuerca) and human evolution during the Middle Pleistocene. In: Bermúdez de Castro, J.M., Arsuaga, J.L., Carbonell, E. (Eds.), Evolución Humana en Europa y los Yacimientos de la Sierra de Atapuerca/Human Evolution in Europe and the Atapuerca Evidence. Junta de Castilla y Leon, Medina del Campo, pp. 283–304.

Arsuaga, J.L., Bermudez, J.M., Carbonell, E., 1997a. The Sima de los Huesos hominid site. J. Hum. Evol. 33 (Special Issue 2/3), 105–421.

Arsuaga, J.L., Carretero, J.M., Lorenzo, C., Gracia, A., Martinez, I., Bermudez de Castro, J.M., Carbonell, E., 1997b. Size variation in Middle Pleistocene humans. Science 277, 1086–1088.

Arsuaga, J.L., Martínez, I., Gracia, A., Lorenzo, C., 1997c. The Sima de los Huesos crania (Sierra de Atapuerca, Spain). A comparative study. J. Hum. Evol. 33, 219–281.

Arsuaga, J.L., Martínez, I., Arnold, L.J., Aranburu, A., Gracia-Tellez, A., Sharp, W.D., Quam, R., Falgueres, C., Pantoja-Perez, A., Bischoff, J., Poza-Rey, E., Parés, J.M., Carretero, J.M., Demuro, M., Lorenzo, C., Sala, N., Martinón-Torres, M., García, N., Alcazar de Velasco, A., Cuenca-Bescós, G., Gómez-Olivencia, A., Moreno, D., Pablos, A., Shen, C.-C., Rodríguez, L., Ortega Martinez, A.I., Garcia, R., Bonmati, A., Bermúdez de Castro, J.M., Carbonell, E., 2014. Neandertal roots: cranial and chronological evidence from Sima de los Huesos. Science 344, 1358–1363.

Arsuaga, J.L., Carretero, J.M., Lorenzo, C., Gomez-Olivencia, A., Pablos, A., Rodriguez, L., Garcia-Gonzalez, R., Bonmati, A., Quam, R., Pantoja-Perez, A., Martinez, I., Aranburu, A., Gracia-Tellez, A., Poza-Rey, E., Sala, N., García, N., Alcazar de Velasco, A., Cuenca-Bescós, G., Bermudez de Castro, J.M., Carbonell, E., 2015. Postcranial morphology of the middle Pleistocene humans from Sima de los Huesos, Spain. PNAS 112, 11524–11529.

Autodesk, Inc, 2012. Autocad. Version 2013. www.autodesk.es.

Bermúdez de Castro, J.M., 1988. Dental remains from Atapuerca/Ibeas (Spain) II. Morphology. J. Hum. Evol. 17, 279–304.

Bermúdez de Castro, J.M., Nicolas, M.E., 1995. Posterior dental size reduction in hominids: the Atapuerca evidence. Am. J. Phys. Anthropol. 96, 335–356.

Bermúdez de Castro, J.M., Martinón-Torres, M., Lozano, M., Sarmiento, S., Muela, A., 2004. Paleodemography of the Atapuerca-Sima de los Huesos hominin sample:

a revision and new approaches to the paleodemography of the European Middle Pleistocene population. J. Anthropol. Res. 60, 5–26.
Bertram, J.E.A., Biewener, A.A., 1988. Bone curvature: Sacrificing Strenght for Load Predictibility? J. Theor. Biol. 131, 75–92.
Bischoff, J.L., Fitzpatrick, J.A., León, L., Arsuaga, J.L., Falguères, C., Bahain, J.J., Bullen, T., 1997. Geology and preliminary dating of the hominid-bearing sedimentary fill of the Sima de los Huesos Chamber, Cueva Mayor of the Sierra de Atapuerca, Burgos, Spain. J. Hum. Evol. 33, 129–154.
Bischoff, J.L., Shamp, D.D., Aranburu, A., Arsuaga, J.L., Carbonell, E., Bermúdez de Castro, J.M., 2003. The Sima de los Huesos hominoids date to beyond U/Th equilibrium (>350 kyr) and perhaps to 400-500 kyr: new radiometric dates. J. Archaeol. Sci. 30, 275–280.
Bonmatí, A., Gómez-Olivencia, A., Arsuaga, J.L., Carretero, J.M., Gracia, A., Martínez, I., Lorenzo, C., Bermúdez de Castro, J.M., Carbonell, E., 2010. Middle Pleistocene lower back and pelvis from an aged human individual from the Sima de los Huesos site. Spain. Proc. Natl. Acad. Sci. 107, 18386–18391.
Boule, M., 1911. L' Homme Fossile de La Chapelle aux Saints. Masson et C. Editeurs, Paris.
Carretero, J.M., 1994. Estudio del esqueleto de las dos cinturas y el miembro superior de los homínidos de la Sima de los Huesos, Sierra de Atapuerca, Burgos. Ph.D. Dissertation, Universidad Complutense, Madrid.
Carretero, J.M., Arsuaga, J.L., Lorenzo, C., 1997. Clavicles, scapulae and humeri from the Sima de los Huesos site (Sierra de Atapuerca, Spain). J. Hum. Evol. 33, 357–408.
Carretero, J.M., Lorenzo, C., Arsuaga, J.L., 1999. Axial and appendicular skeleton of *Homo antecessor*. J. Hum. Evol. 37, 459–499.
Carretero, J.M., Arsuaga, J.L., Martinez, I., Quam, R., Lorenzo, C., Gracia, A., Ortega Martinez, A.I., 2004. Los humanos de la Sima de los Huesos (Sierra de Atapuerca) y la evolución del cuerpo en el género *Homo*. In: Baquedano-Perez, E., Rubio-Jara, S. (Eds.), Miscelanea en Homenaje a Emiliano Aguirre, Museo Arqueologico Regional de Alcalá de Henares Alcalá de Henares, Vol. III, pp. 120–135.
Carretero, J.M., Rodríguez, L., García, R., Gómez, A., Arsuaga, J.L., 2005. Upper limb long bones from Sima de los Huesos site (Sierra de Atapuerca, Burgos, Spain). Am. J. Phys. Anthropol. 126, 84.
Carretero, J.M., Rodriguez, L., García-González, R., Arsuaga, J.L., Gómez-Olivencia, A., Lorenzo, C., Bonmati, A., Gracia, A., Martinez, I., Quam, R., 2012. Stature estimation from complete long bones in the Middle Pleistocene humans from the Sima de los Huesos, Sierra de Atapuerca (Spain). J. Hum. Evol. 62, 242–255.
Churchill, S.E., 1994. Human upper body evolution in the Eurasian Later Pleistocene. Ph.D. Dissertation, University of New Mexico.
Churchill, E., Rhodes, J.A., 2009. The evolution of the human capacity for "killing at a distance": the human fossil evidence for the evolution of projectile weaponry. In: Hublin, J.J., Richards, M. (Eds.), The Evolution of Hominin Diets: Integrating Approaches to the Study of Palaeolithic Subsistence. Springer, Dordrecht, pp. 206–216.
Churchill, E., Holliday, T., Carlson, K.J., Jashashvili, T., Macias, M.E., Mathews, S., Sparling, T., Schimd, P., Ruiter, D.J., Berger, L.R., 2013. The upper limb of *Australopithecus sediba*. Science 340, 12334771–12334776.
Cuenca-Bescós, G., García, N., 2007. Biostratigraphic succession of the early and middle Pleistocene mammal faunas of the Atapuerca cave sites (Burgos, Spain). CFS 259, 99–100.
De Groote, I., 2011. The Neanderthal lower arm. J. Hum. Evol. 61, 396–410.
Frost, H.M., 1973. Orthopaedic Biomechanics. Charles C Thomas, Springfield, Ill.
Galtés, I., Jordana, X., Cos, M., Malgosa, A., Manyosa, J., 2008. Biomechanical model of pronator efficiency: new insight into skeletal adaptation of the hominoid upper limb. Am. J. Phys. Anthropol 135, 293–300.
Galtes, I., Jordana, X., Malgosa, A., Manyosa, J., 2009. Technical Note: forearm pronation efficiency analysis in skeletal remains. Am. J. Phys. Anthropol. 140, 589–594.
García, N., Arsuaga, J.L., Torres, T., 1997. The carnivore remains from the Sima de los Huesos Middle Pleistocene site (Sierra de Atapuerca, Spain). J. Hum. Evol. 33, 155–174.
Gómez-Olivencia, A., Carretero, J.M., Arsuaga, J.L., Rodríguez, L., García-González, R., Martínez, I., 2007. Metric and morphological study of upper cervical spine from the Sima de los Huesos site (Sierra de Atapuerca, Burgos, Spain). J. Hum. Evol. 53, 6–25.
Gorjanović-Kramberger, D., 1906. Der diluviale Mensch von Krapina in Kroatien: ein Beitrag zur Paläoanthropologie. CW Kreidel, Wiesbaden.
Heim, J.L., 1982. Les Hommes Fossiles de la Ferrassie. Masson, Paris.
Holliday, T.W., 1999. Brachial and crural indices of European Late Upper Paleolithic and Mesolithic humans. J. Hum. Evol. 36, 549–566.
IBM Corp Released, 2012. IBM SPSS Statistics for Windows, Version 21.0. IBM Corp, Armonk, NY.
Johanson, D.C., Lovejoy, C.O., Kimbel, W.H., White, T.D., Ward, S.C., Bush, M.E., Latimer, B.M., Coppens, I., 1982. Morphology of the Pliocene partial hominid skeleton (A.L. 288–1) from the Hadar Formation. Ethiopia. Am. J. Phys. Anthropol. 157, 403–451.
Kapandji, A.I., 1999. Fisiología articular: miembro superior. Editorial Medica Panamericana, Madrid.
Keppel, G., 1991. Design and Analysis: A Researcher's Handbook, 3rd ed. Prentice-Hall, Inc, Englewood Cliffs.
Lanyon, L.E., 1980. The influence of function on the development of bone curvature. An experimental study on the rat tibia. J. Zool. 192, 457–466.
Lorenzo, C., 2007. Evolución de la mano en los homínidos. Análisis morfológico de los fósiles de la Sierra de Atapuerca, Depto. Prehistoria. Ph.D. Dissertation, Universidad Complutense de Madrid.
Lorenzo, C., Carretero, J.M., Arsuaga, J.L., Gracia, A., Martínez, I., 1998. Intrapopulational body size variation and cranial capacity variation in Middle Pleistocene Humans: the Sima de los Huesos sample (Sierra de Atapuerca, Spain). Am. J. Phys. Anthropol. 106, 19–33.
Lozano, M., Mosquera, M., Bermúdez de Castro, J.M., Arsuaga, J.L., Carbonell, E., 2009. Right handedness of *Homo heidelbergensis* from Sima de los Huesos (Atapuerca, Spain) 500,000 years ago. Evol. Hum. Behav. 30, 369–376.
Maia Neto, M.A., 1957. Estudo osteometrico do antebraço nos Portugueses. Contrib. Estud. Antropol. Portuguesa. 6, 144–216.
Martin, R., Saller, K., 1957. Lehrbuch der Anthropologie. Gustav Fischer Verlag, Stuttgart.
Martínez, I., Arsuaga, J.L., 1997. The temporal bones from Sima de los Huesos Middle Pleistocene site (Sierra de Atapuerca, Spain). A phylogenetic approach. J. Hum. Evol. 33, 283–318.
Martinón-Torres, M., Bermúdez de Castro, J.M., Gómez-Robles, A., Prado-Simon, L., Arsuaga, J.L., 2012. Morphological description and comparison of the dental remains from Atapuerca-Sima de los Huesos site (Spain). J. Hum. Evol. 62, 7–58.
Materialise, N.V., 2009. Mimics version 13. www.materialise.be.
Max, J., 1960. Quantizing for minimum distortion. Trans. IRE Inform. Theory 6, 7–12.
McCown, T., Keith, A., 1939. The Stone Age of Mount Carmel. Volume II: The Fossil Human Remains from the Levalloiso-Mousterian. Claredon, Oxford.
Pablos, A., Martínez, I., Lorenzo, C., Gracia, A., Sala, N., Arsuaga, J.L., 2013. Human talus bones from the Middle Pleistocene site of Sima de los Huesos (Sierra de Atapuerca, Burgos, Spain). J. Hum. Evol. 65, 79–92.
Pablos, A., Martínez, I., Lorenzo, C., Sala, N., Gracia-Tellez, A., Arsuaga, J.L., 2014. Human calcanei from the Middle Pleistocene site of Sima de los Huesos (Sierra de Atapuerca, Burgos, Spain). J. Hum. Evol. 76, 63–76.
Packard, G.C., Boardman, T.J., 1999. The use of percentages and size-specific indices to normalize physiological data for variation in body size: wasted time, wasted effort. Comp. Biochem. Physiol. Part A 122, 37–44.
Pearson, O.M., Grine, F.E., 1997. Re-analysis of the hominid radii from Cave of Hearths and Klasies River Mouth, South Africa. J. Hum. Evol. 32, 557–592.
Rosas, A., Bastir, M., Martínez-Maza, C., Bermúdez de Castro, J.M., 2002. Sexual dimorphism in the Atapuerca-SH hominids: the evidence from the mandibles. J. Hum. Evol. 42, 451–474.
Ruff, C.B., 2008. Biomechanical analyses of archaeological human skeleton. In: Katzenberg, M.A., Saunders, S.R. (Eds.), Biological Anthropology of the Human Skeleton, Second edition. Wiley-Liss, New York, pp. 183–206.
Ruff, C.B., Hayes, W.C., 1983. Cross-sectional geometry of Pecos Pueblo femora and tibiae—a biomechanical investigation: II. Sex, age, side differences. Am. J. Phys. Anthropol. 60, 383–400.
Senut, B., 1981. L'Humerus et ses articulations chez les Hominidés Plio-Pleistocènes. Centre National de la Recherche Scientifique, Paris.
Sládek, V., Trinkaus, E., Hillson, S., Holliday, T., 2000. The People of the Pavlovian. Skeletal Catalogue and Osteometrics of the Gravettian Fossil Hominids from Dolní Vestonice. Academy of Sciences of the Czech Republic, Brno.
Tobias, P.V., 1978. The earliest Transvaal members of the genus *Homo* with another look at some problems of hominid taxonomy and systematics. Z. Morphol. Anthropol. 69, 225–265.
Trinkaus, E., 1981. Neanderthal limb proportions and cold adaptation. In: Stringer, C. (Ed.), Aspects of Human Evolution. Taylor and Francis, London.
Trinkaus, E., 1983. The Shanidar Neandertals. Academic Press, New York.
Trinkaus, E., Churchill, S.E., 1988. Neandertal radial tuberosity orientation. Am. J. Phys. Anthropol. 75, 15–22.
Trinkaus, E., Churchill, S.E., 1999. Diaphyseal cross-sectional geometry of Near Eastern Middle Palaeolithic humans: the humerus. J. Archaeol. Sci. 26, 173–184.
Trinkaus, E., Churchill, S.E., Ruff, C.B., 1994. Postcranial robusticity in *Homo*. II: Humeral bilateral asymmetry and bone plasticity. Am. J. Phys. Anthropol. 93, 1–34.
Trinkaus, E., Ruff, C.B., Churchill, S.E., 1998. Upper limb versus lower limb loading patterns among near Middle Paleolithic hominids. In: Akazawa, T., Aoki, K., Bar-Yosef, O. (Eds.), Neandertals and Recent Humans in Western Asia. Plenum Press, New York, pp. 391–405.
Vandermeersch, B., 1991. La ceinture scapulaire et les membres superieurs. In: Bar Yosef, O., Vandermeersch, B. (Eds.), Le Squelette Mousterien de Kebara 2. CNRS, Paris, pp. 157–178.
Vandermeersch, B., Trinkaus, E., 1995. The postcranial remains of the Régourdou 1 Neandertal: the shoulder and arm remains. J. Hum.Evol. 28, 439–476.
Vleck, E., 1997. Human remains from Pavlov and biological anthropology of the Gravettian human populations of south Moravia. In: Svoboda, J. (Ed.), The Doni Vestonice Studies. Academy of Science of the Czech Republic, Brno.
Ward, C.V., Wallace, I.J., Patel, B.A., Plavcan, J.M., Kirera, F.M., 2015. A large 1.5 million-year-old hominin radius from Koobi Fora, Kenya. Am. J. Phys. Anthropol. 156, 319.
Yasutomi, T., Nakatsuchi, Y., Kioke, H., Uchiyama, S., 2002. Mechanisms of limitation of pronation/supination of the forearm in geometric models of deformities of the forearm bones. Clin. Biomech. 17, 456–463.